FINAL TECHNICAL REPORT

TO

AIR FORCE OFFICE OF SCIENTIFIC RESEARCH

AFOSR GRANT: F49620-95-1-0120

PERIOD COVERED: 1 February 1995- 31 January 1998

TITLE OF PROJECT: Crack Mechanics of Functionally Graded Coating/Substrate Systems

PRINCIPAL INVESTIGATOR: Gang Bao

NAME OF INSTITUTION: The Johns Hopkins University
Charles and 34th Street
Baltimore, MD 21218

REPORT DOCUMENTATION PAGE

AFRL-SR-BL-TR-98-

0834

1. AGENCY USE ONLY *(Leave blank)*	2. REPORT DATE	3. REPORT T
	September 1998	Final Technical Report 1 Feb 95 to 31 Jan 98

4. TITLE AND SUBTITLE
Crack Mechanics of Functionally GRaded Coating/Substrate Systems

5. FUNDING NUMBERS
F49620-95-1-0120
2302/BS

6. AUTHOR(S)
Gang Bao

7. PERFORMING ORGANIZATION NAME(S) AND ADDRESS(ES)
Johns Hopkins University
Charles and 34th Street
Baltimore, MD 21218

8. PERFORMING ORGANIZATION REPORT NUMBER

9. SPONSORING/MONITORING AGENCY NAME(S) AND ADDRESS(ES)
AFOSR/NA
110 Duncan Avenue Suite B115
Bolling AFB, DC 20332-8050

10. SPONSORING/MONITORING AGENCY REPORT NUMBER
F49620-95-1-0120

11. SUPPLEMENTARY NOTES

12a. DISTRIBUTION AVAILABILITY STATEMENT
Approved for public release; distribution unlimited.

12b. DISTRIBUTION CODE

13. ABSTRACT *(Maximum 200 words)*

This 3-year research program focuses on micromechanics and fracture mechanics analyses of cracking in functionally graded coating/substrate systems used in turbine engines and wear-related applications. Functionally graded materials (FGMs) are new advanced composites whose composition varies from place to place according to performance requirements. Recent developments of FGMs have demonstrated that functionally graded materials have the potential to enjoy a wide range of thermal and structural applications including thermal barrier coatings, wear, oxidation and corrosion resistant coatings and metal/ceramic joining. The objectives of the study include: establishing a fundamental understanding of the relationship between coating composition and performance, quantifying the influence of coating gradation, evaluating the effect of metal plasticity and crack bridging, and predicting the fracture driving forces and fracture resistance curves. Emphases in this study is placed on delamination fracture and multiple cracking in FGM coatings. The fundamental understanding gained from this study may enable one to select coatings at the component design stage. The systematic model predictions and design charts for the thermomechanical behavior of the coating/substrate systems may provide guidance to the gradation design of functionally graded coatings. This study thus can have a significant impact on the developments of functionally graded materials in turbine engine and wear related applications.

14. SUBJECT TERMS	15. NUMBER OF PAGES
	6
	16. PRICE CODE

17. SECURITY CLASSIFICATION OF REPORT	18. SECURITY CLASSIFICATION OF THIS PAGE	19. SECURITY CLASSIFICATION OF ABSTRACT	20. LIMITATION OF ABSTRACT
Unclassified	Unclassified	Unclassified	UL

OBJECTIVES:

This 3-year research program focuses on micromechanics and fracture mechanics analyses of cracking in functionally graded coating/substrate systems used in turbine engines and wear-related applications. The objectives of the study include: quantifying the influence of coating gradation, evaluating the effect of metal plasticity and crack bridging, and predicting the fracture driving forces and fracture resistance curves. Emphases is placed on multiple cracking and delamination fracture in coating/substrate systems. The fundamental understanding gained from this study will enable one to select coating gradation at the component design stage.

SUMMARY OF EFFORT:

In the first six months (Feb. 1995 - July 1995), research was conducted to develop micromechanics models for predicting the thermomechanical properties of functionally graded coatings. Coatings of the inclusion/matrix type were considered, with the coating gradation characterized by a power-law type relation. The elastic moduli and thermal expansion coefficient of the coating were predicted in terms of the local volume fractions and thermomechanical properties of the phases in the coating. Distribution of thermal residual stresses in the coating/substrate systems were calculated. A linear fracture mechanics analysis was carried out to calculate the crack driving forces (energy release rates or stress intensity factors) for multiple cracks in the coating under both thermal and mechanical loads.

During the 12-month period of August, 1995 - July 1996, a linear fracture mechanics analysis was carried out to calculate the crack driving forces (energy release rates) for delamination cracks in the coating or at the coating/substrate interface. Multilayered coatings and coatings of the inclusion/matrix type were considered, with the coating gradation characterized by a power-law type relation. A steady-state heat transfer analysis was also performed for the FGM coating/substrate system to calculate the increase of the coating thickness owing to the functional gradation. A crack bridging model was developed for the crack tip shielding effect due to the non-uniform distribution of metal ligaments in the crack wake. The reduction in the fracture driving force owing to crack bridging was quantified.

From August 1996 to July 1997, research was conducted to develop computational models for bridged edge and internal through cracks in functionally graded coating/substrate systems. A singular integral equation approach was taken to solve the boundary value problem in which both the coating and the substrate are assumed to be linear elastic. The crack driving forces of edge and internal cracks in a FGM panel and in a FGM coating/metal substrate system were calculated and the effect of the coating gradation quantified. An analysis was also carried out for cracking in TBC/substrate systems consist of TBC, FGM bond coat, and metal substrate.

During the period of August 1997 - January 1998, an effort was made to predict the fatigue behavior of advanced ceramics and ceramic coatings. A model was developed for fatigue growth of an edge crack in nontransforming ceramics based on a crack bridging analysis. Systematic predictions were made of the effects of initial crack length, load frequency, and the bridging characteristics. This work could be further extended to include the effect of nonuniform distribution of bridging grains.

BRIEF OUTLINE OF RESEARCH FINDINGS:

Functionally graded coatings such as thermal barrier coatings on advanced metals and alloys can sustain multiple cracking upon thermal and mechanical loading. A special feature

pertaining to the fracture behavior of coating is the coating gradation which can be characterized by the local volume fraction of metal. To guide the design of coating gradation so that cracking damage can be minimized, a fracture mechanics study is made of the crack driving force for multiple cracks in functionally graded ceramic/metal coatings. The metal substrate and the ceramic/metal coating are taken as linear elastic, with the elastic properties of the coating varying through the film thickness. Systematic finite element calculations are made for the energy release rate of the cracks in the coating as determined by the coating gradation, crack length, and the crack density; both mechanical and thermal loads are considered. It is found that compared with the pure ceramic coating, gradation of the coating can significantly reduce the crack driving force. It is also found that under mechanical loading the effect of different gradations on the crack driving force is relatively small. However, under thermal loading the influence of coating gradation can be significant.

Delamination cracking is a major damage mode in multilayered composites including FGMs. To quantify such damage, a micromechanics analysis is carried out of delamination cracking in functionally graded coating/substrate systems. The FGM coating is taken to be a ceramic/metal composite with its gradation characterized by the local volume fraction of metal. The elastic properties thus change with position in the coating along the thickness direction. Linear fracture mechanics analyses are made for the strain energy release rate of the delamination crack as determined by the coating gradation, the thickness ratio of the coating/substrate system, and the elastic properties of the ceramic and metal phase. Both the total energy release rate and the stress intensity factors of the system are predicted. The mode mixity can be quantified using the analytical formula developed. Buckling of the FGM coating due to the compressive residual stresses is analyzed based on the thin plate theory; the buckle-driven delamination is modeled accordingly. It is found that functional gradation of the coating has a strong influence on the residual stress distribution, which in turn changes the buckling behavior of the coating. By using a FGM coating, the fracture driving force for the delamination crack can be significantly reduced. A steady-state heat transfer analysis is also performed for the FGM coating/substrate system; the increase of the coating thickness owing to the functional gradation is predicted.

In functionally graded coatings made of layered or particle/matrix type metal-ceramic composites, ligaments of the metal phase often bridge the crack in its wake, exerting a closure force to the crack surfaces, thus reducing the crack tip stress intensity. To quantify this effect, a crack bridging analysis is carried out to predict crack propagation in coatings made of functionally graded materials (FGM). The FGM coating is taken to be a ceramic/metal composite with its gradation characterized by the local volume fractions of metal and ceramic phases. Fracture in the FGM coating is resisted by the plastic deformation of metal ligaments in the crack wake that bridge the crack; the crack bridging, however, is not uniform. A position-dependent crack bridging model is developed taking into account the coating gradation and metal plasticity. The model is subsequently used in a finite element analysis to predict the reduced fracture driving force. It is found that crack bridging in the FGM coating can significantly reduce the crack tip stress intensity. It is also found that coating gradation has a strong influence on the fracture driving force and the crack length at arrest. The present finite element model can be extended readily to study the effect of large-scale plastic deformation on crack growth in a FGM coating.

Due to the performance requirements of high temperature applications of functionally graded coating/metal substrate systems, most of the FGM coatings are ceramic-rich near the coating surface. It is therefore necessary to analyze fracture of edge cracks in FGM coatings. A special feature pertaining to the fracture behavior of such coatings is the position-dependent crack bridging owing to the metal ligaments in the crack wake. To guide the design of coating gradation so that cracking damage can be minimized, a fracture mechanics study is made of the crack driving force for bridged edge cracks in functionally graded ceramic/metal coatings using

a singular integral equations approach. The metal substrate and the ceramic/metal coating are taken as linear elastic, with the elastic properties of the coating varying through the film thickness. The crack density is assumed to be relatively small such that the crack-crack interactions can be neglected. Calculations are made for the stress intensity factors at the tip of the cracks in the coating as determined by the coating gradation, crack length, the bridging characteristics, and the applied load. It is found that crack bridging can significantly reduce the crack driving force. It is also found that the gradation of the coating affects the crack driving force through an interplay between the elastic properties of the coating and the crack bridging characteristics. Such an interplay is systematically quantified.

To guide the design of thermal barrier coatings (TBCs) for advanced turbine engines, a micromechanics analysis is carried out for delamination cracking in TBCs consisting of a ceramic top coating, a functionally graded bond coat, and a metal substrate. The FGM bond coat is taken to be a multilayered ceramic/metal composite with its thermomechanical properties changing along the thickness direction of the coating. The energy release rate of the delamination crack is determined analytically as a function of the coating gradation, the location of the crack, the thickness ratios of the coating/substrate system. Finite element calculations have also been performed to give energy release rate of the crack when the crack length is relatively small. As observed experimentally, cracks perpendicular to the interface may initiate in the top ceramic coating and propagate into the bond coat; the driving force of such cracks are quantified using a finite element methods. It is found that it is quite beneficial to use a FGM bond coat. However, it is remain to be seen how the functionally gradation would affect the resistance of the coating to oxidation.

In order to predict the fatigue behavior of advanced ceramics and ceramic coatings such as alumina, silicon carbide and silicon nitride, a model is developed for fatigue growth of an edge crack in nontransforming ceramics based on a large-scale crack bridging analysis. The crack bridging is assumed to be owing to grain boundary sliding, and the fatigue behavior of the ceramics is modeled using a frictional wear law that accounts for the shielding degradation. Under cyclic loading conditions, the fatigue problem is analyzed by solving a set of singular integral equations. It is found that the competition between shielding degradation and shielding accumulation results in a modified Paris' law. It is also found that the dependence on the maximum crack tip stress intensity can be very strong, but that on the R-ratio is only moderate. Systematic predictions are made of the effects of initial crack length, load ratio, and the bridging characteristics. The models developed can be further extended to include the effect of nonuniform distribution of bridging grains.

PERSONNEL SUPPORTED:

G. Bao, Associate Professor.

H. Cai, Graduate Research Assistant. Awarded M.S.E. May 1995; awarded Ph.D. May 1996.

H. Zhao, Graduate Research Assistant. Awarded M.S.E. May 1997; Ph.D. expected October 1998.

PUBLICATIONS:

1) G. Bao and R. Wang, "Multiple cracking in functionally graded ceramic/metal coatings", *Int. J. Solids Structures* **32**, 2853-2871 (1995).

2) J. Rohde, S. Schmauder, and G. Bao, "Mesoscopic modeling of gradient zones in hardmetals", *Computational Materials Science* **7**, 63-67 (1996).

3) G. Bao and H. Cai, "Delamination cracking in functionally graded coating/metal substrate systems", *Acta Mater.* **45**, 1055-1066 (1997).

4) H. Cai and G. Bao, "Crack bridging in functionally graded coatings", *Int. J. Solids Structures* **35**, 701-717 (1998)..

5) H. Zhao and G. Bao, "A note on solving fracture problems using a singular integral equation approach", to be submitted to *J. Appl. Mech.* (1998).

6) H. Zhao and G. Bao, "Crack problems in FGM strips and coatings", to be submitted to *Int. J. Solids Structures* (1998).

7) H. Zhao and G. Bao, "Large-scale bridging analysis of fatigue crack growth in grain-bridging ceramics", to be submitted to *Acta Mater.*(1998).

INTERACTIONS:

- I gave a talk titled "Fracture in functionally graded coating/substrate systems" at the Engineering Foundation Conference on Mechanics & Physics of Layered & Graded Materials in Davos, Switzerland in August 1995.
- Professor K. Kokini at Purdue University and I organized a symposium on mechanics of ceramics and ceramic composites including functionally graded materials for the ASME International Mechanical Engineering Congress & Exposition in San Francisco, CA in Nov. 1995. I also gave a talk on delamination cracking in functionally graded ceramic/metal coatings at the symposium.
- I worked with Professor S. Schmauder at University of Stuttgard, Germany on multiple cracking in functionally graded coating for hard-metal tools.
- I have discussed with Dr. T.J. Chuang at NIST with regard to the experimental measurements of cracking in functionally graded TBC performed by his group and the potential collaborations.
- I have discussed with Prof. T. Nakamura at the University of New York, Stony Brook on the development of fracture mechanics models for functionally graded TBC.
- I have been collaborating with Dr. David Walls at Pratt&Whitney on the life prediction of components made of fiber reinforced MMCs. We have discussed how to extend the work to include functionally graded TBC.
- I have discussed with Dr. Tim Weihs at the Department of Materials Science and Engineering, The Johns Hopkins University about the design and fabrication of multilayered FGM TBCs.
- I gave an invited talk, "Crack bridging in functionally graded materials", at the ASME International Mechanical Engineering Congress & Exposition in Atlanta, GA in Nov. 1996.
- While on my sabbatical leave at the Institute of Materials Research and Engineering (IMRE), the National University of Singapore, I have been discussing with Prof. L.C. Lim, the Program Director of the Advanced Materials and Composites Program on developing collaborations between Hopkins and IMRE on functionally graded materials for high temperature applications.
- I attended the AFOSR Mechanics of Composite Materials Program Review Meeting at Dallas, TX, Nov. 1997 and gave an invited talk, "Crack mechanics of functionally graded coating/substrate systems".
- I gave an invited seminar, "Fracture mechanics analysis of functionally graded materials", at the Nanyang University of Technology, Singapore in February 1998.

- I gave an invited seminar, "Micromechanics of deformation and damage in heterogeneous materials", at Ecole Centrale Paris, CNRS Laboratory of Mechanics and Materials, Paris, France in May 1998.
- I attended the Workshop on Mechanics of Materials, Ecole Centrale Paris, Paris, France in May 1998 and gave an invited talk, "Delamination and multiple cracking in functionally graded coating/substrate systems".
- I will give an invited talk "Fracture analysis of functionally graded coating/substrate systems", at the Symposium on Failure Characterization of Interfaces and Functionally Graded Materials, ASME 1998 IMECE, Anaheim, CA, Nov. 1998.
- I will give a talk "Analyses of fracture in FGM layers and coatings", at the ASME Ceramic Coatings Symposium, ASME 1998 IMECE, Anaheim, CA, Nov. 1998.

Pergamon

PII: S1359-6454(96)00232-7

Acta mater. Vol. 45, No. 3, pp. 1055–1066, 1997

Published by Elsevier Science Ltd

1359-6454/97 $17.00 + 0.00

DELAMINATION CRACKING IN FUNCTIONALLY GRADED COATING/METAL SUBSTRATE SYSTEMS

G. BAO and H. CAI

Department of Mechanical Engineering, The Johns Hopkins University, Baltimore, MD 21218, U.S.A.

(Received 8 May 1996; accepted 18 June 1996)

Abstract—A micromechanics analysis is carried out for delamination cracking in functionally graded coating/substrate systems. The FGM coating is taken to be a ceramic/metal composite with its thermomechanical properties changing with position in the coating along the thickness direction. Based on a linear fracture mechanics analysis, the energy release rate of the delamination crack is determined as a function of the coating gradation, the location of the crack, the thickness ratio of the coating/substrate system, and the elastic properties of the ceramic and metal phases. Formulae are given for the stress intensity factors and the mode mixity of the system. Buckling of the FGM coating due to compressive residual stresses is analyzed using a thin plate theory; the buckle-driven delamination is modeled accordingly. It is found that functional gradation of the coating can significantly reduce the fracture driving force of the delamination crack in both edge-delamination and buckle-driven delamination cases. A steady-state heat transfer analysis is performed for the FGM coating/substrate system; the increase of the coating thickness owing to the functional gradation is quantified. *Copyright © 1997 Acta Metallurgica Inc.*

1. INTRODUCTION

A functionally graded material (FGM) is a composite whose composition varies from place to place according to performance requirements. For example, a FGM coating may have pure ceramic at the surface and pure metal at the coating/substrate interface. Recent development of FGM has demonstrated that such materials have the potential to enjoy a wide range of thermal and structural applications, including thermal gradient structures, wear and corrosion resistant coatings and metal/ceramic joining [1, 2].

Functional gradation opens a new avenue for optimizing both material and component structures to achieve high performance and material efficiency; it also posts many challenging mechanics problems in the theoretical and experimental determination of the microstructure-property relationships, and in correlating design, processing and performance of FGMs [3].

To establish the fundamental relationship between material gradation and thermomechanical properties of FGMs, extensive studies have been carried out of the effective properties [4, 5], thermal stress distributions [6–8] and fracture in functionally graded materials [9–13]. In particular, the fracture mechanics analysis of Erdogan and associates has been extended by Noda and Jin to include thermal load [14–16], and by Bao and Wang [17] to include the effects of different material gradation. Experimental observations of cracking in FGMs have been made by several investigators, including surface crack initiation in thermal barrier coatings [18] and multiple cracking in a $NiAl–Al_2O_3$ FGM layer under bending [19]. The present work focuses on the delamination cracking in FGM coating/substrate systems.

Ceramic coatings have been developed for use in thermal gradient structures, automotive engines and cutting and grinding tools to protect the surfaces from melting, wear, corrosion and oxidation. However, due to thermal expansion mismatch between the coating and substrate, delamination cracking and coating spalling can occur upon experiencing thermal cycling and mechanical loading, causing premature failure of the component [20]. Similar damage mechanisms exist in other compressed films [21]. Extensive mechanics studies on delamination and spalling in film/substrate systems, with both the film and substrate being homogeneous, have been carried out [22–25]. A review of the mechanics models for delamination cracking in such systems can be found in Hutchinson and Suo [26].

To alleviate the problems encountered in using the pure ceramic coatings, functionally graded materials have been developed for use as thermal barrier coatings (TBC) and as protective coatings for hard-metal tools [27]. FGM coatings have the potential to simultaneously reduce thermal expansion mismatch, increase interface bonding strength, and enhance coating toughness. To realize this potential, an effort is made in the present study to establish the relationship between delamination cracking of the coating and coating gradation, aiming to provide

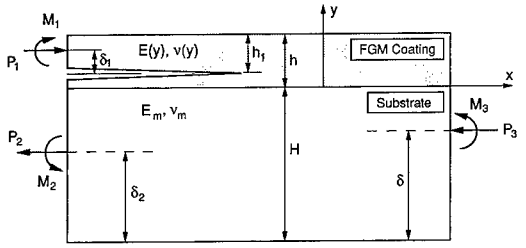

Fig. 1. A schematic of delamination cracking in a functionally graded coating/metal-substrate system under applied forces and moments.

guidance to both the coating design and the life prediction of the FGM coating/substrate systems.

2. PRELIMINARIES

Consider a functionally graded ceramic/metal coating on a homogeneous, isotropic metal substrate, as shown schematically in Fig. 1. The coating is taken to be a ceramic of an inclusion/matrix type shown in Fig. 2(a), or a functionally graded multilayer depicted in Fig. 2(b). Based on the performance requirements for thermal barrier coatings and coatings in wear-related applications, in this study, only coatings that are ceramic-rich near the coating surface and metal-rich near the coating/substrate interface are considered. For convenience, the y-axis is set along the coating thickness direction, the x-axis lies within the coating/substrate interface, as illustrated in Fig. 1. At any position y in the ceramic/metal coating, the local volume fraction of ceramic is assumed to be $g(y)$ which can be used to characterize the coating gradation. Generally speaking, $g(y)$ can be any non-singular, non-negative function of y. To gain insight, it is assumed that $g(y)$ obeys a pure power-law type relation

$$g(y) = (y/h)^m \tag{1}$$

where h is the coating thickness, and m is a material parameter. The gradation given in equation (1) implies that the coating always has 100% ceramic at the surface (i.e. $g(h) = 1$) and 100% metal at the interface. Though idealized, the coating gradation defined in equation (1) can be used to model approximately the FGM coatings of both the inclusion/matrix type shown in Fig. 2(a), and the multilayered type shown in Fig. 2(b). The total volume fraction f_c of ceramic in the FGM coating is related to the exponent m in equation (1) by

$$f_c = 1/(m+1). \tag{2}$$

The coating gradation given in equation (1) is similar to that used by Drake *et al.* [7] and Bao and Wang [17] in their studies of FGM systems.

Due to the heterogeneous nature of a functionally graded material, it is quite difficult to obtain the exact solution of the effective elastic moduli and thermal expansion coefficient of a FGM coating in terms of the relative volume fractions and thermomechanical properties of the metal and ceramic phases. For a FGM coating in the inclusion/matrix type (Fig. 2(a)), the existing micromechanical cell models are no longer valid since no unit cell containing a single particle can be used to represent the whole composite body. For a FGM with a layered structure as that depicted in Fig. 2(b), the existing micromechanical cell models are valid only if the thickness of each individual layer is much larger than the average particle size.

As a first-order approximation, in this study Young's modulus $E(y)$ and thermal expansion coefficient $\alpha(y)$ of the FGM coating are assumed to have power-law type expressions

$$E(y) = E_m + (E_c - E_m)\left(\frac{y}{h}\right)^n \tag{3a}$$

$$\alpha(y) = \alpha_m + (\alpha_c - \alpha_m)\left(\frac{y}{h}\right)^r \tag{3b}$$

where E_m and E_c are Young's moduli, and α_m and α_c the thermal expansion coefficients of the metal and ceramic phases, respectively, and n and r are exponents determined by the coating gradation.

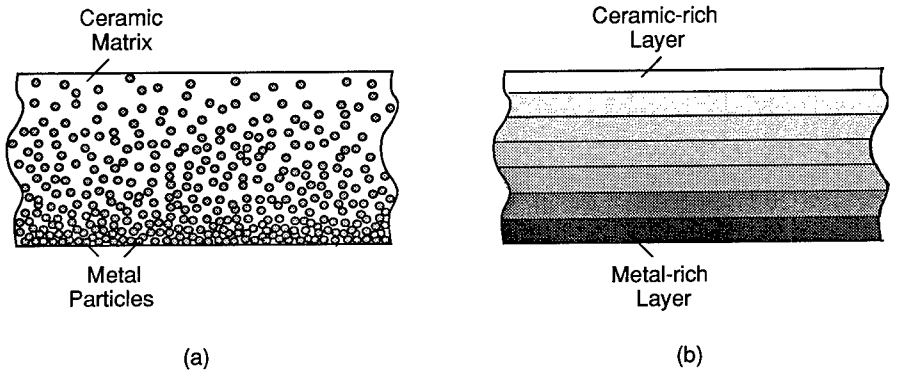

Fig. 2. Typical microstructures of functionally graded coatings; (a) an inclusion/matrix structure; (b) a multilayered structure.

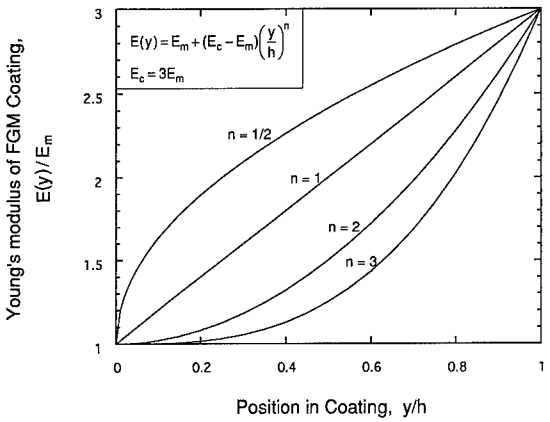

Fig. 3. Young's modulus of the coating as a function of position as determined using a power-law type model with different gradation exponent.

Shown in Fig. 3 are curves for $E(y)/E_m$ as a function of y/h for $E_c/E_m = 3$ for $n = 0.5$, 1 and 2. Note that $n = r = 0$ corresponds to a pure ceramic coating. For simplicity, in the case studies, it is assumed that Poisson's ratios of the metal and ceramic are the same, i.e.

$$\nu_m = \nu_c = \nu. \tag{4}$$

Practically, the exponents n and r in equations (3a) and (3b) can be determined from measurements of the position-dependent Young's modulus and the thermal expansion coefficient of the FGM coating. They can also be obtained approximately from the predictions of Young's modulus and the thermal expansion coefficient of the FGM coating using a micromechanics cell model [28, 29] in conjunction with the coating gradation (1). Although Poisson's ratios of the metal and ceramic phases are usually different, and Poisson's ratio of the FGM coating varies with position, the effect of using equation (4) as an approximation is expected to be small.

3. EDGE DELAMINATION

As depicted in Fig. 1, the FGM coating/metal substrate system containing an edge delamination crack is assumed to be in plane strain conditions and subjected to axial loads (force per unit width) P_1, P_2, P_3 and bending moments (moment per unit width) M_1, M_2 and M_3. Both the FGM coating and the metal substrate are taken to be isotropic, linear elastic, with Young's moduli $E(y)$, E_m and Poisson's ratio $\nu(y)$, ν_m for the coating and substrate, respectively; plasticity of the metal phase and the possible crack bridging mechanisms are neglected. The crack, which is located a distance h_1 from the coating surface, has length a much larger than the coating thickness h. Attention in this study is restricted to situations where $h_1 \leqslant h$, although the same approach can be used for $h_1 > h$. When $h_1 = h$, the delamination crack lies within the interface between the coating and the substrate. Note that the thermomechanical properties of the coating defined in equations (3) and (4) have no discontinuities within the coating nor at the interface $y = 0$. The delamination crack, therefore, can be analyzed without introducing the complex stress intensity factor [30]. However, the fracture toughness of the interface may still be lower than that of the metal substrate owing to the deposition process.

3.1. General results

The energy release $\mathcal{G}$ of the delamination crack can be derived using an elementary beam theory [25]. Assuming that the three edges have linear strain distributions, the positions of the neutral axes δ_1, δ_2 and δ (Fig. 1) can be determined by

$$\delta_1 = \frac{\lambda_1}{\lambda_0} - (h - h_1) \tag{5}$$

$$\delta_2 = \frac{H}{2} + \frac{2(\omega_1 - \lambda_1) + H(\omega_0 - \lambda_0)}{2(\bar{E}_m H + \omega_0 - \lambda_0)} \tag{6}$$

$$\delta = \frac{H}{2} + \frac{2\omega_1 + H\omega_0}{2(\bar{E}_m H + \omega_0)} \tag{7}$$

where H is the thickness of the substrate, $\bar{E}_m = E_m/(1 - \nu_m^2)$ is the plane strain Young's modulus of the metal substrate,

$$\lambda_0 = \int_{h-h_1}^{h} \bar{E}(y)\, dy \tag{8a}$$

$$\lambda_1 = \int_{h-h_1}^{h} \bar{E}(y) y\, dy \tag{8b}$$

$$\omega_0 = \int_{0}^{h} \bar{E}(y)\, dy \tag{9a}$$

$$\omega_1 = \int_{0}^{h} \bar{E}(y) y\, dy \tag{9b}$$

where $\bar{E}(y) = E(y)/[1 - \nu^2(y)]$ is the plane strain Young's modulus of the FGM coating. Since $a \gg h$, the energy release rate is simply the difference of the strain energy per unit length per unit width stored in the edges far behind and far ahead of the crack tip

$$\mathcal{G} = \frac{P_1^2}{2\lambda_0} + \frac{M_1^2}{2(\lambda_2 - \lambda_1^2/\lambda_0)} + \frac{P_2^2}{2(\omega_0 - \lambda_0 + H\bar{E}_m)} + \frac{M_2^2}{2(\phi_2 + \phi_m)} - \frac{P_3^2}{2(\omega_0 + H\bar{E}_m)} - \frac{M_3^2}{2(\psi_2 + \psi_m)} \tag{10}$$

where

$$\lambda_2 = \int_{h-h_1}^{h} \bar{E}(y) y^2\, dy \tag{11a}$$

$$\phi_2 = (H - \delta_2)^2(\omega_0 - \lambda_0) + 2(H - \delta_2)(\omega_1 - \lambda_1) + \omega_2 - \lambda_2 \tag{11b}$$

$$\psi_2 = (H-\delta)^2\omega_0 + 2(H-\delta)\omega_1 + \omega_2 \quad (11c)$$

with

$$\omega_2 = \int_0^h \bar{E}(y)y^2\,dy \quad (11d)$$

and

$$\phi_m = \frac{\bar{E}_m}{3}[(H-\delta_2)^3 + \delta_2^3] \quad (12a)$$

$$\psi_m = \frac{\bar{E}_m}{3}[(H-\delta)^3 + \delta^3]. \quad (12b)$$

The expression of $\mathcal{G}$ given in equation (10) can be further simplified using a superposition scheme [25],

$$\mathcal{G} = \frac{1}{2\bar{E}_m}\left[\frac{P^2}{Uh} + \frac{M^2}{Vh^3} + \frac{2PM}{\sqrt{UV}h^2}\sin\gamma\right] \quad (13)$$

where

$$P = P_1 - C_1P_3 - C_2M_3/h \quad (14a)$$

$$M = M_1 - M_3C_3 \quad (14b)$$

with

$$C_1 = \frac{\lambda_0}{\omega_0 + H\bar{E}_m} \quad (15a)$$

$$C_2 = \frac{h[\lambda_1 + (H-\delta)\lambda_0]}{\psi_2 + \psi_m} \quad (15b)$$

$$C_3 = \frac{\lambda_2 - \lambda_1^2/\lambda_0}{\psi_2 + \psi_m} \quad (15c)$$

The non-dimensional parameters U, V and $\sin\gamma$ in (13) are given by

$$\frac{1}{U} = \bar{E}_m h\left[\frac{1}{\lambda_0} + \frac{1}{\omega_0 - \lambda_0 + H\bar{E}_m} + \frac{(H-\delta_2+\lambda_1/\lambda_0)^2}{\phi_2+\phi_m}\right] \quad (16a)$$

$$\frac{1}{V} = \bar{E}_m h^3\left[\frac{1}{\lambda_2 - \lambda_1^2/\lambda_0} + \frac{1}{\phi_2+\phi_m}\right] \quad (16b)$$

$$\frac{\sin\gamma}{\sqrt{UV}} = \frac{\bar{E}_m h^2(H-\delta_2+\lambda_1/\lambda_0)}{\phi_2+\phi_m}. \quad (16c)$$

It is readily shown that for a homogeneous coating, the expressions in equation (10), (15) and (16) are identical to those given in Suo [25].

The delamination crack shown in Fig. 1 is, of course, a mixed-mode crack. The stress intensity factors K_I and K_{II} can be derived from equation (13) based on linearity and dimensionality,

$$K_I = \frac{P}{\sqrt{2hU}}\cos\omega + \frac{M}{\sqrt{2h^3V}}\sin(\omega+\gamma) \quad (17a)$$

$$K_{II} = \frac{P}{\sqrt{2hU}}\sin\omega - \frac{M}{\sqrt{2h^3V}}\cos(\omega+\gamma) \quad (17b)$$

where ω is a function of the thickness ratio h/H, the location of the crack h_1/h, and the material properties of the FGM coating and the substrate. Once ω is given, the stress intensity factors, and the phase angle ψ

$$\psi = \tan^{-1}\left(\frac{K_{II}}{K_I}\right) \quad (18)$$

can be fully determined.

3.2. Total energy release rate

The results given in equations (5)–(17) are valid for a FGM coating with any elastic moduli $E(y)$ and $\nu(y)$. To gain insight, in the following, we assume that $E(y)$ has a power-law form, equation (3a),

$$E(y) = E_m + (E_c - E_m)\left(\frac{y}{h}\right)^n \quad (3a)$$

and that Poisson's ratio of the FGM coating is constant ($=\nu_m$). Consequently, the parameters λ_0, λ_1, λ_2, ω_0, ω_1 and ω_2 defined in equations (8), (9) and (11) can be expressed in a closed-form; they are for $\ell = 1, 2$ and 3,

$$\lambda_{\ell-1} = \bar{E}_m h^\ell\left[\frac{1}{\ell}\left(1-\left(1-\frac{h_1}{h}\right)^\ell\right) + \left(\frac{E_c}{E_m}-1\right)\left(\frac{1-(1-h_1/h)^{n+\ell}}{n+\ell}\right)\right] \quad (19a)$$

$$\omega_{\ell-1} = \bar{E}_m h^\ell\left[\frac{1}{\ell} + \left(\frac{E_c}{E_m}-1\right)\left(\frac{1}{n+\ell}\right)\right]. \quad (19b)$$

The strain energy release rate $\mathcal{G}$ of the delamination crack is a function of the applied loads, and the geometric and material parameters. In a non-dimensional form, we have

$$\frac{\mathcal{G}\bar{E}_m}{\sigma^2 h} = \phi\left(\frac{h_1}{h}, \frac{H}{h}, \frac{E_c}{E_m}, n\right) \quad (20)$$

where ϕ is a non-dimensional function, σ is a stress measure related to the applied loads but not dependent on the parameters in ϕ. For any FGM coating on a homogeneous substrate subjected to applied loads P_1, P_2, P_3 and M_1, M_2, M_3 as shown in

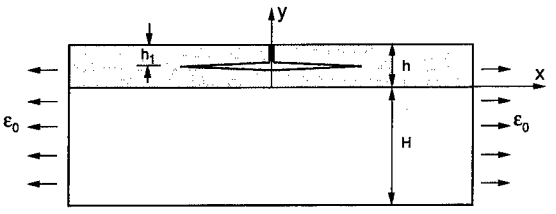

Fig. 4. A schematic of delamination cracking in a functionally graded coating/metal-substrate system under far-field uniform straining.

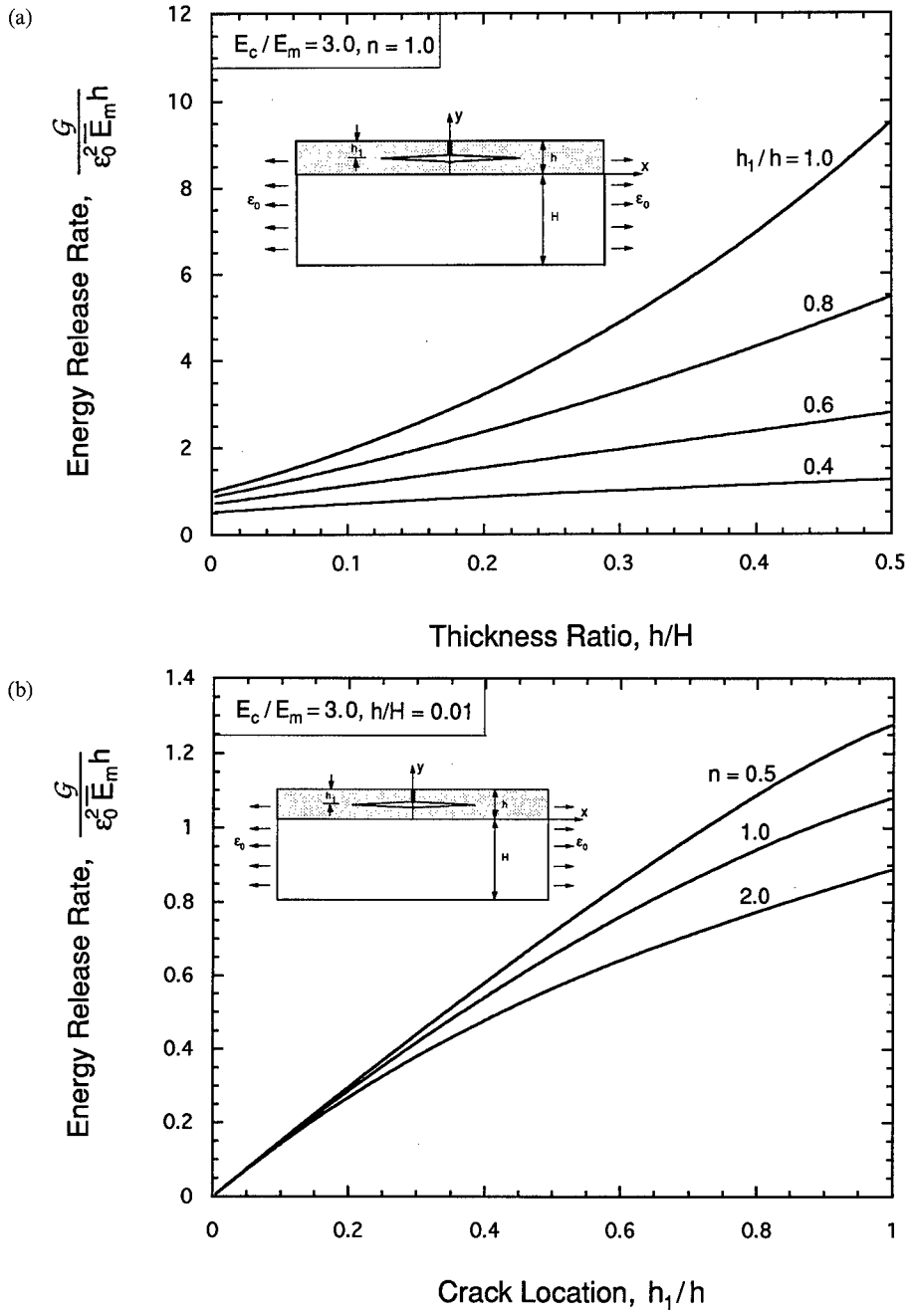

Fig. 5. (a) The normalized energy release rates $\mathcal{G}$ as a function of the thickness ratio h/H for a crack with location $h_1/h = 0.4, 0.6, 0.8$ and 1.0; (b) $\mathcal{G}$ as a function of the crack location h_1/h for the gradation exponent $n = 0.5$, 1.0 and 2.0 for $h/H = 0.01$.

Fig. 1, ϕ can be calculated readily using the above equations.

To illustrate the trends in the normalized $\mathcal{G}$ in equation (20), consider the FGM coating/metal substrate system subjected to a uniform applied strain ϵ_0, as shown in Fig. 4. We have in this case

$$P = \epsilon_0 \lambda_0, \quad M = 0 \tag{21}$$

and the stress σ in (20) can be taken as $\sigma = \epsilon_0 \bar{E}_m$. Displayed in Fig. 5(a) is the normalized energy release rate as a function of the thickness ratio h/H for $E_c/E_m = 3$, $n = 1$ for $h_1/h = 0.4, 0.6, 0.8$ and 1.0. It is seen that the total strain energy release rate $\mathcal{G}$ increases with increasing thickness ratio h/H. Further, with a fixed h/H, $\mathcal{G}$ increases with increasing h_1/h. Clearly, the location of the delamination crack depends on $\mathcal{G}$ as well as the toughness Γ of the FGM layer which is also a function of position. When the FGM coating is ceramic-rich at the surface and metal-rich at the coating/substrate interface, Γ is

expected to be higher near the interface. Consequently, the delamination crack is likely to be located some distance away from the interface. To show the effect of material gradation, in Fig. 5(b), the normalized $\mathcal{G}$ is plotted against the relative location of the crack h_1/h for $E_c/E_m = 3$, $h/H = 0.01$ for $n = 0.5$, 1 and 2. The fracture driving force is lower when n is larger, as can be seen from Fig. 5(b).

3.3. *Stress intensity factors*

The stress intensity factors K_I and K_{II} of the delamination crack can be calculated using equation (17) if the parameter ω is known. When the gradation of the FGM coating obeys equation (3a), ω is a function of the thickness ratio H/h, crack location h_1/h, and material parameters E_c/E_m and n, i.e.

$$\omega = \omega\left(\frac{h_1}{h}, \frac{H}{h}, \frac{E_c}{E_m}, n\right). \tag{22}$$

To quantify ω, a finite element analysis was carried out using the commercial code ABAQUS for the FGM coating/metal substrate system depicted in Fig. 1. The FGM coating is divided into 200 layers, the first layer in the coating away from the interface is assumed to have the same Young's modulus as of the metal matrix. For $n = 1, 2, \ldots, 99$, the $(2n)$th and $(2n + 1)$th layers have the same Young's modulus $E(y_n)$ with $y_n = 0.01nh$. The delamination crack in the FGM coating is assumed to be located in-between $(2n)$th and $(2n + 1)$th layers; complications due to the oscillatory singular crack-tip fields of an interface crack is thus avoided. Shown in Fig. 6 is an example of the finite element mesh for the FGM coating. Clearly, in this finite element model the gradation is not continuous, nor is it in the real material. This model mimics the microstructure of a fine multilayered FGM coating, or an inclusion/matrix type FGM coating with gradation $E(y)$ given in equation (3a). The stress intensity factors K_I and K_{II} were determined through the calculated crack opening displacements [33]. The accuracy of the calculated K_I and K_{II} was assessed by taking the coating as homogeneous and comparing the resulting K-values with that obtained by Suo [25].

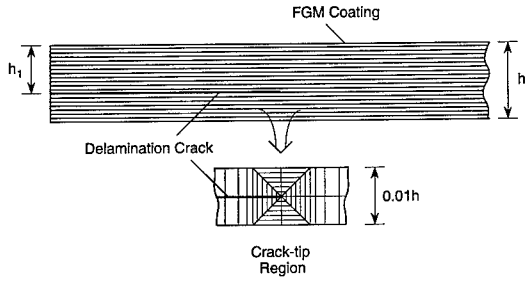

Fig. 6. A typical finite element mesh used in calculating the stress intensity factors of a delamination crack in the functionally graded coating.

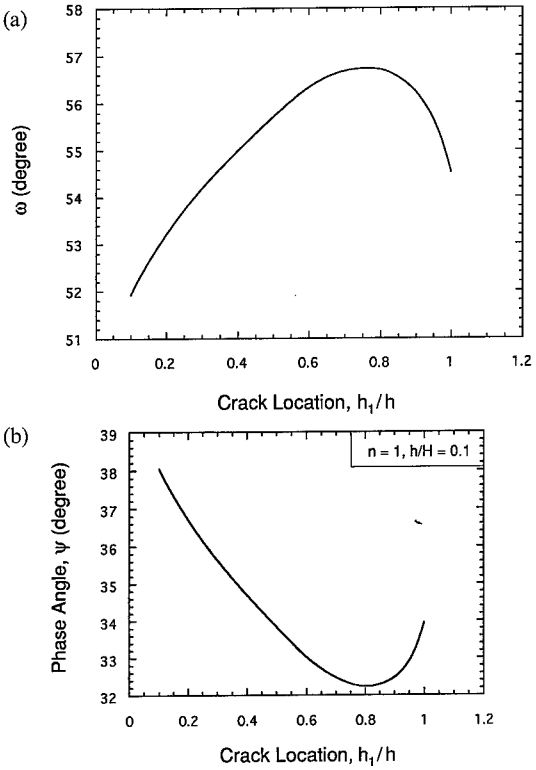

Fig. 7. The parameter ω shown in (a) and phase angle ψ shown in (b) as a function of crack location h_1/h for a FGM coating/metal substrate system with $n = 1$, $h/H = 0.1$.

Shown in Fig. 7(a) is ω as a function of the relative location of the crack h_1/h for $H/h = 10$, $E_c/E_m = 3$, $n = 1$. With less than 1% error, the curve for ω shown in Fig. 7(a) can be represented by

$$\omega = 51.308 + 6.688(h_1/h) + 13.038(h_1/h)^2 - 16.301(h_1/h)^3. \tag{23}$$

The corresponding phase angle of the delamination crack, $\psi = \tan^{-1}(K_{II}/K_I)$ is plotted in Fig. 7(b). It is interesting to note that the minimum value of ψ occurs at $h_1/h = 0.8$ which implies that, if the coating has a constant toughness and if fracture is locally mode-I controlled, the delamination crack will be at $h_1 = 0.8h$.

As a limiting case, the delamination crack located at the coating/substrate interface (i.e. $h_1 = h$) is analyzed using a finite element method and the corresponding function ω is obtained. Displayed in Fig. 8(a) is ω as a function of the thickness ratio $\eta = h/H$ for $n = 0.5$, 1.0 and 2.0. The points are the finite element results; the solid lines are the curve-fittings. It is seen that for different values of n, ω can be represented approximately as a linear function of h/H. Shown in Fig. 8(b) are ω vs $1/n$ curves for $H/h = 1.0$, 2.0, 3,0, 4.0, 5.0 and 10.0.

Within a few percent error, these curves can be reproduced by

$$\omega = \omega_0(n) - (3 + 1/n)(h/H) \tag{24a}$$

$$\omega_0(n) = 52.1 - 7.31/n + 15.264/n^2 - 4.894/n^3. \tag{24b}$$

The stress intensity factors for a crack located at the coating/substrate interface can be calculated using equations (17) and (24).

4. BUCKLE-DRIVEN DELAMINATION

Delamination cracking often occurs at the coating/substrate interface when the coating buckles due to the compressive thermal residual stress [26]. This buckle-driven delamination cracking can also occur in a FGM coating/metal substrate system, although the residual stress is somewhat reduced. A new feature for the FGM system is that the delamination crack may be located in the coating away from the interface, since at the interface the residual stress is lower and the toughness can be much higher than

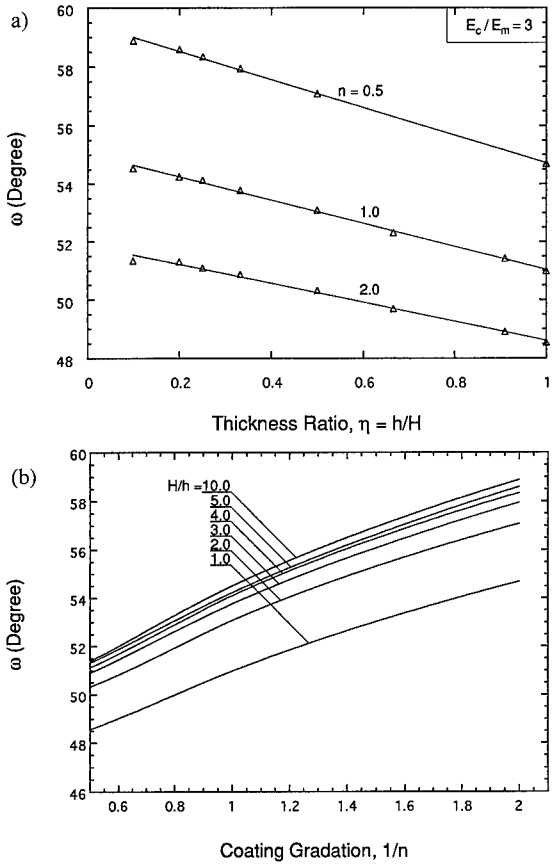

Fig. 8. (a) The parameter ω as a function of the thickness ratio h/H for the gradation exponent $n = 0.5$, 1.0 and 2.0; (b) the parameter ω as a function of the coating gradation exponent n for thickness ratio $H/h = 1.0$, 2.0, 3.0, 4.0, 5.0, and 10.0. The delamination crack is located at the coating/substrate interface.

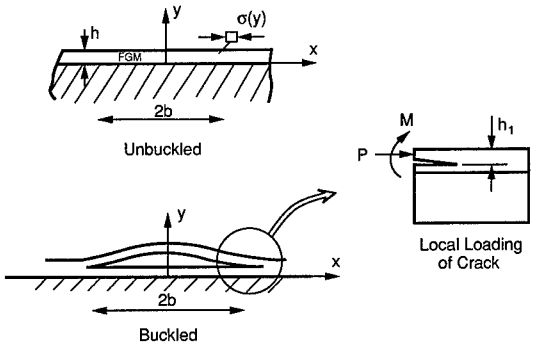

Fig. 9. A schematic of a buckle-driven delamination crack in a FGM coating on an infinitely deep metal substrate.

that at other places in the FGM coating. Attention in this paper is restricted to the case in which the thickness of the substrate is much larger than that of the coating, i.e. $h/H \to 0$. This will greatly simplify the buckling analysis of the film.

Consider an one-dimensional blister shown in Fig. 9. The FGM coating is assumed to contain a debonded region of width $2b$ located a distance h_1 from the coating surface. Under an equi-biaxial compressive in-plane stress $\sigma_{xx} = \sigma_{zz} = \sigma$ (e.g. a thermal residual stress), the debonded region may buckle up, inducing a plane strain, mixed mode delamination crack. The energy release rate $\mathcal{G}$ of the delamination crack can be obtained by analyzing the local loads P and M on the buckled film, then inserting them into equation (13).

To calculate the loading of the delamination crack, it is assumed that $h_1 \ll b$ so that the debonded region shown in Fig. 9 can be represented by a wide, clamped Eular column of width $2b$. Following Hutchinson and Suo [26], the displacement v of the film in the y-direction is governed by

$$\bar{D}\frac{d^4v}{dx^4} - (P - N_r)\frac{d^2v}{dx^2} = 0 \tag{25}$$

where P is the change in the resultant force in film due to buckling, N_r is the resultant force owing to the thermal residual stress, and $\bar{D}$ the bending stiffness

$$\bar{D} = \int_{h-h_1}^{h} (y - h + h_1 - \delta_1)^2 \bar{E}(y)\, dy = \lambda_2 - \lambda_1^2/\lambda_0. \tag{26}$$

Solving equation (25) with the boundary conditions

$$v|_{x=\pm b} = 0, \quad \left.\frac{dv}{dx}\right|_{x=\pm b} = 0 \tag{27}$$

and taking the lowest non-zero eigen-value, we have

$$v(x) = \tfrac{1}{2}\xi h\left[1 + \cos\frac{\pi x}{b}\right] \tag{28a}$$

where [26]

$$\xi = \frac{v(0)}{h} = \frac{4}{\bar{h}}\left[\frac{\bar{D}}{\lambda_0}\left(\frac{N_r}{N_c} - 1\right)\right]^{1/2} \tag{28b}$$

with

$$N_c = \frac{\pi^2 \bar{D}}{b^2}. \tag{28c}$$

The loading P and M can be given readily from the above solution

$$P = N_r - N_c \tag{29a}$$

$$M = \frac{\pi^2 \bar{D} h}{2b^2}\,\xi \tag{29b}$$

The energy release rate of the buckle-driven delamination crack is then obtained from (13)

$$\mathcal{G} = \frac{N_r^2}{2\lambda_0}\left(1 - \frac{N_c}{N_r}\right)\left(1 + 3\frac{N_c}{N_r}\right). \tag{30}$$

The thermal residual stress distribution in a FGM system can be calculated readily once the thermo-mechanical properties of the coating and the substrate are given [31]. As mentioned earlier, in this study we assume that the variation of both Young's modulus $E(y)$ and the thermal expansion coefficient $\alpha(y)$ in the FGM coating obeys a power-law type relation defined by equation (3). Further, Poisson's ratio of the coating is taken to be constant ($=\nu_m$). Based on these assumptions, the residual stress distribution in the FGM coating is given by

$$\sigma_r(y) = \frac{E(y)\Delta T[\alpha_m - \alpha(y)]}{1 - \nu_m} \tag{31}$$

where ΔT is the temperature change. Typically $\Delta T < 0$ and, for a FGM metal/ceramic coating, $\alpha(y) \leqslant \alpha_m$; $\sigma_r(y)$ in equation (31) is therefore compressive. The resultant force N_r owing to the thermal residual stress is

$$N_r = \int_{h-h_1}^{h} \sigma_r(y)\,dy$$

$$= \frac{E_m(\alpha_m - \alpha_c)h\Delta T}{1 - \nu_m}\left[\frac{1}{r+1}\left(1 - \left(1 - \frac{h_1}{h}\right)^{r+1}\right)\right.$$

$$\left. + \frac{1}{n+r+1}\left(\frac{E_c}{E_m} - 1\right)\left(1 - \left(1 - \frac{h_1}{h}\right)^{r+n+1}\right)\right]. \tag{32}$$

Plotted in Fig. 10 are curves of the normalized energy release rate $\mathcal{G}/\mathcal{G}_0$ against non-dimensional temperature drop $\Delta T/\Delta T_c = N_r/N_c$ for $E_c/E_m = 3$, $r = n = 1$ for $h_1/h = 0.2, 0.4, 0.6, 0.8$ and 1.0. The reference energy rate $\mathcal{G}_0$ is given by

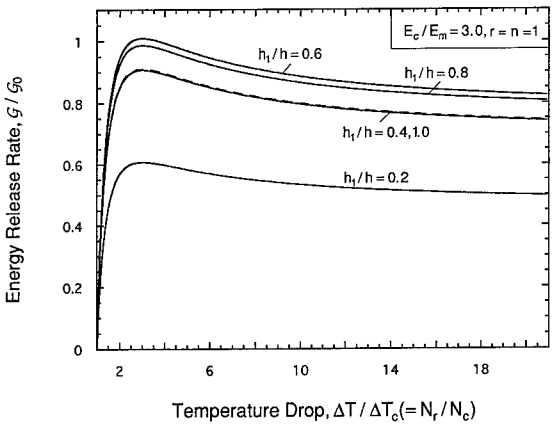

Fig. 10. The normalized energy release rate of a buckle-driven delamination crack as a function of the temperature drop for crack locations $h_1/h = 0.2, 0.4, 0.6, 0.8$ and 1.0. Note that the energy release rates for $h_1/h = 0.4$ and $h_1/h = 1.0$ are almost identical.

$$\mathcal{G}_0 = \frac{\sigma_0^2 h}{2\bar{E}_m}, \quad \sigma_0 = \frac{E_m(\alpha_m - \alpha_c)\Delta T}{1 - \nu_m}. \tag{33}$$

The critical temperature drop ΔT_c is the temperature drop at which the film buckles

$$\Delta T_c = \frac{\pi^2 \bar{D}(1 - \nu_m)}{E_m(\alpha_m - \alpha_c)hb^2}\left[\frac{1}{r+1}\left(1 - \left(1 - \frac{h_1}{h}\right)^{r+1}\right)\right.$$

$$\left. + \frac{1}{n+r+1}\left(\frac{E_c}{E_m} - 1\right)\left(1 - \left(1 - \frac{h_1}{h}\right)^{r+n+1}\right)\right]^{-1}. \tag{34}$$

It is noteworthy that when a crack is located at $h_1/h = 0.6$ the fracture driving force is higher than

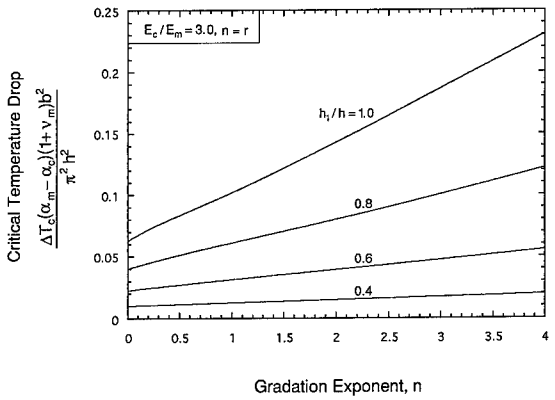

Fig. 11. The nondimensional critical temperature drop as a function of the gradation exponent n for a buckle-driven delamination crack with location $h_1/h = 0.4, 0.6, 0.8$ and 1.0.

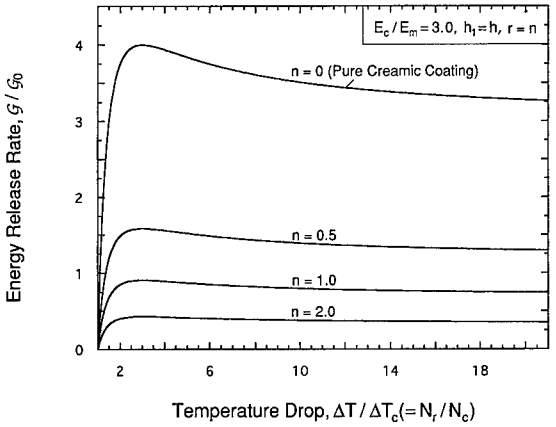

Fig. 12. The normalized energy release rate of a buckle-driven delamination crack as a function of the temperature drop for coating gradation exponent $n = 0, 0.5, 1.0$ and 2.0. The crack is located at the coating/substrate interface. Note that $n = 0$ corresponds to a pure ceramic coating.

that with other crack locations. The curve with $h_1/h = 0.4$ is almost identical to that with $h_1/h = 1.0$. For each curve, the peak value of $\mathcal{G}$ occurs at $\Delta T/\Delta T_c = 3.0$.

The critical temperature drop ΔT_c is an important design parameter for if $\Delta T < \Delta T_c$, no buckling of the film will occur. Shown in Fig. 11 is the non-dimensional temperature drop as a function of the gradation exponent n for $E_c/E_m = 3$, $n = r = 1$ for $h_1/h = 0.4, 0.6, 0.8$ and 1.0. It is seen that the change of ΔT_c with n is almost linear. Since increasing n implies to increase the total volume fraction of metal in the FGM coating, the trend in ΔT_c vs n curves shown in Fig. 11 might be expected. Note also that when $n = 0$, the FGM coating becomes a pure ceramic coating, so the critical temperature drop is the smallest for all values of h_1/h. When the delamination crack is located near the interface, the film is thicker than otherwise; ΔT_c is thus higher. The opposite is true when the crack is located near the coating surface. Clearly, for a fixed temperature drop (e.g. from the processing temperature to room temperature), initial flaws in the FGM coating located near the coating surface are more likely to cause local buckling.

The use of a FGM ceramic/metal coating can significantly decrease the residual compressive stresses in the coating, thus reducing the possibility of buckle-driven delamination. To illustrate, in Fig. 12, the normalized energy release rate $\mathcal{G}/\mathcal{G}_0$ is plotted against non-dimensional temperature drop $\Delta T/\Delta T_c$ $(= N_r/N_c)$ for $E_c/E_m = 3$, $r = n$, $h_1 = h$ for $n = 0.0, 0.5, 1.0$ and 2.0. Note that with increasing n, the energy release rate decreases, since the volume fraction of metal in the coating increases. For a pure ceramic coating ($n = 0$), the fracture driving force is much higher than that for a FGM coating, as can be seen from Fig. 12.

5. STEADY-STATE HEAT TRANSFER

As shown clearly in the previous section, with a FGM coating the buckle-driven delamination crack can have a much lower fracture driving force compared with a pure ceramic coating. However, the FGM coating contains metal phase which may have a much higher thermal conductivity. Consequently, when the FGM coating is used as a thermal barrier coating, to provide the same degree of protection to the metal substrate, a thicker coating has to be used.

To predict the thickness of a FGM coating as determined by the heat shielding requirements and the coating gradation, consider the FGM coating/metal substrate system shown in Fig. 13. It is assumed that the working temperature (e.g. the temperature of gas in the engine) on the coating surface is T_0, and the temperature the metal substrate can sustain is T_m. For simplicity, T_0 is assumed to be constant; for a conservative design it can be taken as the maximum gas temperature at coating surface. Further, the coating thickness h is taken to be much smaller than other dimensions of the system so that the edge effects can be neglected. The resulting one-dimensional steady-state heat transfer problem is governed by

$$\dot{Q} = -k(y)\frac{dT}{dy} \tag{35}$$

where $T(y)$ is the temperature distribution in the coating, $\dot{Q}$ is the heat flux per unit area, and $k(y)$ is the thermal conductivity of the FGM coating. Integration of equation (35) gives

$$T_0 - T_m = -\dot{Q}\int_0^h \frac{dy}{k(y)}. \tag{36}$$

For a pure ceramic coating with the same surface temperatures and heat flux, we have

$$T_0 - T_m = -\frac{\dot{Q}h_c}{k_c} \tag{37}$$

where h_c is the thickness and k_c the thermal conductivity of the ceramic coating. Combining

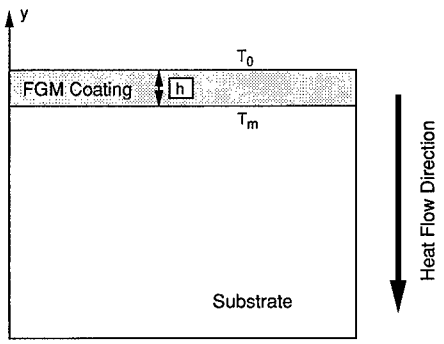

Fig. 13. A schematic of the steady-state heat transfer problem for a FGM coating/metal substrate system.

equation (36) and (37) leads to

$$\frac{h_c}{h} = k_c \int_0^1 \frac{ds}{k(s)} \tag{38}$$

where $s = y/h$. It is interesting to note that the thickness ratio h/h_c only depends on the thermal conductivities of the FGM coating and the ceramic. Obviously, for a pure ceramic coating, $k(s) = k_c$, $h = h_c$; for a ceramic/metal FGM coating, $k(s) > k_c$, $h > h_c$ which implies that when a thermal barrier coating is made of functionally graded material, a thicker coating needs to be used.

The thermal conductivity k of a dual-phase composite with spherical inclusions uniformly distributed in the matrix is given by [32]

$$k = k_m \left[1 + \frac{c}{(1-c)/3 + k_m/(k_i - k_m)} \right] \tag{39}$$

where the subscripts i and m represent the inclusion and matrix phases, respectively, and c is the volume fraction of the inclusion. For a FGM coating, however, the definitions of "matrix" and "inclusion" are position dependent: near the surface of the coating the ceramic phase is the matrix and the metal phase is in the form of inclusion, while near the coating/substrate interface, the opposite is true. At the middle of the coating (the percolation area) the ceramic and metal phases are both continuous; matrix and inclusion cannot be well defined. Further, for a FGM coating the inclusion phase, be it ceramic or metal, is not uniformly distributed in the matrix. The expression given in equation (39) is a good approximation only for a multi-layered coating with inclusion size much smaller than the thickness of each layer.

To gain insight, in this study, we assume that up to the percolation limit equation (39) can still be used to obtain the effective thermal conductivity k of the FGM coating. The local volume fraction g of the ceramic phase, however, is a function of the position y in the coating. We further assume that at the percolation limit g_p, there is a sudden change in the effective thermal conductivity, as shown in Fig. 14. Specifically, when $g(y) < g_p$, the metal phase is the matrix,

$$k(y) = k_m \left[1 + \frac{g(y)}{[1+g(y)]/3 + k_m/(k_c - k_m)} \right]. \tag{40}$$

When $g(y) > g_p$, the ceramic phase becomes the matrix,

$$k(y) = k_c \left[1 + \frac{1-g(y)}{[g(y)]/3 + k_c/(k_m - k_c)} \right]. \tag{41}$$

The percolation limit g_p of a metal/ceramic composite is typically ranging from 0.4 to 0.6, depending on the specific microgeometry of the

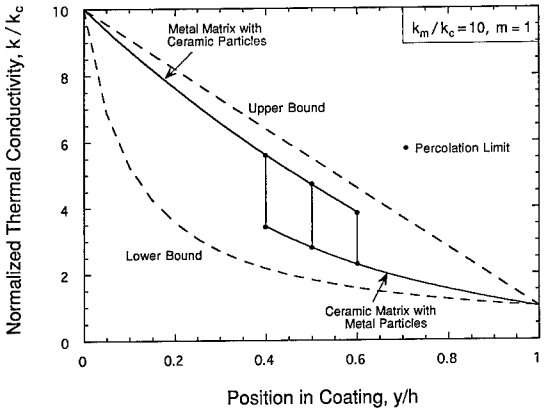

Fig. 14. The effective thermal conductivity of the FGM coating as a function of the position in the coating for $k_m/k_c = 10$. The local volume fraction of ceramic in the coating is characterized by $g(y) = (y/h)^m$. The solid lines are the predictions obtained using the composite spheres model; the dashed line are upper and lower bounds based on the rule of mixtures. Three percolation limits ($g_p = 0.4$, 0.5 and 0.6) are considered.

phases. To simplify the analysis, three values of g_p are considered: $g_p = 0.4$, 0.5 and 0.6. Displayed in Fig. 14 is the thermal conductivity of the FGM coating as a function of the position y in the coating corresponding to a pure power-law gradation

$$g(y) = (y/h)^m. \tag{1}$$

Also shown in Fig. 14 are the upper and lower bounds of $k(y)$ obtained using the rule of mixtures,

$$k_{upper} = g(y)k_c + [1 - g(y)]k_m$$
$$k_{lower} = \{g(y)/k_c + [1 - g(y)]/k_m\}^{-1}. \tag{42}$$

Having obtained the effective thermal conductivity of the FGM coating, the thickness ratio h/h_c can be predicted readily using equations (1) and (38) in conjunction with equation (40) and (41). Plotted in

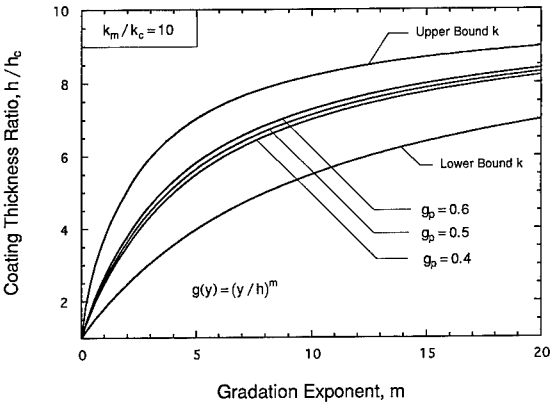

Fig. 15. Predictions of the coating thickness ratio h/h_c as a function of the coating gradation exponent m based on the effective thermal conductivity of the FGM coating obtained using different approaches. The $g_p = 0.5$ curve provides a good estimate of the coating thickness as compared with that of a pure ceramic coating.

Fig. 15 is the thickness ratio h/h_c as a function of the coating gradation exponent m for $k_m/k_c = 10$ for $g_p = 0.4$, 0.5 and 0.6. Shown also are h/h_c vs m curves corresponding to the upper and lower bounds of the effective thermal conductivity of the coating given in equation (42). Indeed the metal phase in the FGM coating could result in a significantly thicker coating compared with the pure ceramic coating. Note that the coating gradation exponent m is related to the total volume fraction of metal f_m by

$$f_m = m/(1 + m). \tag{43}$$

For example, with $g_p = 0.5$, when $m = 1$, $f_m = 0.5$, $h/h_c = 2.641$; when $m = 9$, $f_m = 0.9$, $h/h_c = 7.149$. Typically $0.5 \leqslant m \leqslant 2$, i.e. $0.333 \leqslant f_m \leqslant 0.667$, the thickness ratio of the FGM coating is thus $1.882 \leqslant h/h_c \leqslant 3.734$. It is also seen from Fig. 15 that the effect of different percolation limits g_p on h/h_c is very small. Consequently, the $g_p = 0.5$ curve provides a good approximation for predicting the thickness of the FGM coating.

6. CONCLUDING REMARKS

Functionally graded coatings are potentially very attractive to a number of applications including as thermal barrier coatings and wear resistant coatings. Compared with pure ceramic coatings, FGM coatings can have relatively high hardness and oxidation resistance at the surface, but with much lower thermal residual stresses. The material gradation in such coatings provides a new dimension in optimizing the coating performance. However, due to material gradation, the FGM coating is inherently heterogeneous, and the microstructure–performance relationship is quite complex since more material parameters come into play. It is therefore critical to develop mechanics models that can guide both the microstructural design of a functionally graded material and the design of components made of FGM.

In order to realize the potential of FGM coatings, this paper focuses on delamination cracking and steady-state heat transfer in the FGM coating/metal substrate system, aiming to gain a better understanding of the microstructure–performance relationship. Both the coating and the substrate are taken as linear-elastic, with the coating gradation characterized by position-dependent Young's modulus and thermal expansion coefficient. An edge delamination crack in the coating is analyzed first using a simple beam theory, with the crack plane parallel to, but not necessarily on, the coating/substrate interface. Formulae for the energy release rate and stress intensity factors of the crack are obtained for a FGM coating with arbitrary gradation; their dependence on the thickness ratio h/H, crack location h_1/h and gradation exponent n is illustrated for FGM coating with Young's modulus and thermal expansion coefficient obeying a power-law type position dependence.

Buckle-driven delamination in a FGM coating on an infinitely deep metal substrate is analyzed based on a plate theory; the critical temperature drop at the onset of buckling and the energy release rate of the delamination crack are determined in terms of the position-dependent thermomechanical properties of the coating and the location of the crack. It is found that the use of FGM coating can significantly reduce the likelihood of local buckling and the fracture driving force, since the thermal residual compressive stresses in a FGM coating can be much lower. However, by performing a steady-state heat transfer analysis, it is found that when the FGM coating is used as a thermal barrier coating, the thickness of the coating needs to be increased in order to provide the same degree of protection to the metal substrate.

The delamination cracking analysis conducted in this study is based on a number of assumptions. For example, the crack plane is taken to be parallel to the interface. In reality, however, the crack may be tilted. Further, plasticity of metal in the FGM coating may play a very important role in delamination cracking; such an effect is neglected in the present study but will be quantified in future studies. Although under far-field uniform tensile straining the crack driving force is found to be larger when the crack is at the interface, the true location of the crack is likely to be away from the interface since the toughness of the FGM coating is also higher near the interface. Modeling the position-dependent fracture toughness of a FGM coating is thus crucial.

Acknowledgement—This work was supported by AFOSR though a research grant F49620-95-1-0120 to G. Bao.

REFERENCES

1. H. Takahashi and T. Hashida, *JSME Int. J.* **33,** 281 (1990).
2. A. Mortensen and S. Suresh, *Int. Mater. Rev.* **40,** 239 (1995).
3. A. J. Markworth, K. S. Ramesh and W. P. Parks Jr, *J. mater. Sci.* **30,** 2183 (1995).
4. J. Aboudi, S. M. Arnold and M. J. Pindera, *Composites Engng* **4,** 1 (1994).
5. G. Dvorak and J. Zuiker, *Composites Engng* **4,** 19 (1994).
6. R. L. Williamson, B. H. Rabin and J. T. Drake, *J. appl. Phys.* **74,** 1310 (1993).
7. J. T. Drake, R. L. Williamson and B. H. Rabin, *J. appl. Phys.* **74,** 1321 (1993).
8. A. E. Giannakopoulos, S. Suresh, M. Finot and M. Olsson, *Acta metall. mater.* **43,** 1335 (1994).
9. F. Erdogan, *J. Appl. Mech.* **52,** 823 (1985).
10. F. Delale and F. Erdogan, *J. appl. Mech.* **50,** 609 (1983).
11. F. Delale and F. Erdogan, *J. appl. Mech.* **55,** 317 (1988).
12. F. Erdogan and B. H. Wu, *Ceramic Transactions*, Vol. 34, Functionally Gradient Materials (edited by J. B. Hole *et al.*), pp. 39–46. American Ceramic Society, Westerville, Ohio (1993).
13. P. Gu and R. J. Asaro, *Int. J. Solids Struct.*, submitted.
14. Z. H. Jin and N. Noda, *Int. J. Engng Sci.* **31,** 793 (1993).

15. Z.-H. Jin and N. Noda, *Int. J. Solids Struct.* **31,** 203 (1994).
16. N. Noda and Z.-H. Jin, *Int. J. Solids Struct.* **30,** 1039 (1993).
17. G. Bao and L. Wang, *Int. J. Solids Struct.* **32,** 2853 (1995).
18. K. Kokini and Y. Takeuchi, *J. Therm. Stress.* **17,** 63 (1994).
19. J. J. Lannutti, *Composites Engng* **4,** 81 (1994).
20. R. A. Miller and C. E. Lowell, *Thin Solid Films* **99,** 265 (1982).
21. A. G. Evans and J. W. Hutchinson, *Int. J. Solids Struct.* **20,** 455 (1984).
22. M. D. Thouless, A. G. Evans, M. F. Ashby and J. W. Hutchinson, *Acta metall.* **35,** 1406 (1987).
23. M. D. Drory, M. D. Thouless and A. G. Evans, *Acta metall.* **36,** 2019 (1988).
24. H. M. Jensen, J. W. Hutchinson and K. S. Kim, *Int. J. Solids Struct.* **26,** 1099 (1990).
25. Z. Suo, *J. appl. Mech.* **57,** 627 (1990).
26. J. W. Hutchinson and Z. Suo, *Advances in Applied Mechanics* (edited by J. W. Hutchinson and T. Y. Wu), Vol. 29, pp. 63–191 Academic Press (1991).
27. J. Rohde, S. Schmauder and G. Bao, *Comput. Mater. Sci.*, submitted.
28. Z. Hashin, *J. appl. Mech.* **29,** 143 (1962).
29. R. M. Christensen and K. H. Lo, *J. mech. Phys. Solids* **27,** 315 (1979).
30. J. R. Rice, *J. appl. Mech.* **55,** 98 (1988).
31. L. B. Freund, *J. Cryst. Growth* **132,** 341 (1993).
32. R. M. Christensen, *Mechanics of Composite Materials*. Krieger, Malabar, FL (1991).
33. G. Bao, B. Fan and A. G. Evans, *Mech. Mater.* **13,** 59 (1992).

Pergamon

Int. J. Solids Structures Vol. 35, No. 7–8, pp. 701–717, 1998

0020–7683/98 $19.00 + .00

PII: S0020–7683(97)00082–6

CRACK BRIDGING IN FUNCTIONALLY GRADED COATINGS

H. CAI and G. BAO†
Department of Mechanical Engineering, The Johns Hopkins University, Baltimore, MD 21218, U.S.A.

(*Received* 12 *July* 1996; *in revised form* 24 *February* 1997)

Abstract—A crack bridging analysis is carried out to predict crack propagation in coatings made of functionally graded materials (FGM). The FGM coating is taken to be a ceramic/metal composite with its gradation characterized by the local volume fractions of metal and ceramic phases. Fracture in the FGM coating is resisted by the plastic deformation of metal ligaments in the crack wake that bridge the crack; the crack bridging, however, is not uniform. A position-dependent crack bridging model is developed taking into account the coating gradation and metal plasticity. The model is subsequently used in a finite element analysis to predict the reduced fracture driving force. It is found that crack bridging in the FGM coating can significantly reduce the crack tip stress intensity. It is also found that coating gradation has a strong influence on the fracture driving force and the crack length at arrest. The present finite element model can be extended readily to study the effect of large-scale plastic deformation on crack growth in a FGM coating. © 1997 Elsevier Science Ltd

1. INTRODUCTION

Functionally graded materials (FGMs) have the potential to enjoy a wide range of thermal and structural applications, including thermal gradient structures, wear and corrosion resistant coatings and metal/ceramic joining (Takahashi and Hashida, 1990; Mortensen and Suresh, 1995). To establish the fundamental relationship between material gradation and thermomechanical properties of FGMs, extensive studies have been carried out of the effective properties (Aboudi *et al.* 1994; Dvorak and Zuiker, 1994; Aboudi *et al.* 1995), deformation and stress distributions (Williamson *et al.*, 1993; Drake *et al.*, 1993; Giannakopoulos *et al.*, 1995; Finot and Suresh, 1996) and fracture in functionally graded materials (Erdogan, 1985; Delale and Erdogan, 1983, 1988; Erdogan and Wu, 1993; Chen and Erdogan, 1996). In particular, the fracture mechanics analysis of Erdogan and associates has been extended by Noda and Jin to include thermal load (Jin and Noda, 1993; Noda and Jin, 1993; Jin and Noda, 1994), and by Bao and Wang (1995) and Bao and Cai (1996) to include the effects of different material gradation. Experimental observations of cracking in FGMs have been made by several investigators, including surface crack initiation in thermal barrier coatings (Kokini and Takeuchi, 1994) and multiple cracking in a NiAl-Al_2O_3 FGM layer under bending (Lannutti, 1994).

Ceramic, metal and polymer coatings have been widely used in various industries, from aerospace to automobile to microelectronics, to enhance the performance. In particular, ceramic coatings have been developed for use in thermal gradient structures, automotive engines and cutting and grinding tools to protect the surfaces from melting, wear, corrosion and oxidation. However, due to thermal expansion mismatch between the coating and substrate, multiple cracking and coating spalling can occur upon experiencing thermal cycling and mechanical loading, causing premature failure of the component. The use of functionally graded coatings has the potential to simultaneously reduce thermal expansion mismatch, increase interface bonding strength, and enhance coating toughness. To realize this potential, a systematic micromechanics study was carried out by Bao and Wang (1995) of multiple cracking in functionally graded ceramic/metal coatings. Systematic finite element calculations were made for the energy release rate of the cracks in the coating as

† Correspondence address: Department of Mechanical Engineering, The Johns Hopkins University, 125 Latrobe Hall 3400 N. Charles St., Baltimore MD 21218-2686, U.S.A.

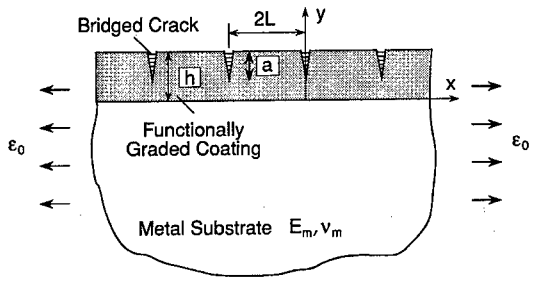

Fig. 1. A schematic of bridged multiple cracks in a functionally graded coating/metal-substrate system.

determined by the coating gradation, crack length, and the crack density; both mechanical and thermal loads were considered. However, in their study, the influence of crack bridging and metal plasticity in the functionally graded coatings was neglected.

Crack bridging is a very common phenomenon in the fracture of composites (Bao and Suo, 1992). For example, in a unidirectional ceramic fiber reinforced metal matrix composite, fibers can bridge the matrix crack, reducing the crack-tip stress intensity, and increasing significantly the fatigue life of the component (Walls *et al.*, 1993; Bao and McMeeking, 1994, 1995). When a ceramic/metal FGM coating is of the inclusion/matrix type, the metal particles in the ceramic matrix can bridge the crack, thus enhance the fracture resistance of the coating. The fracture behavior of ductile-particle reinforced brittle matrix composites has been analyzed (e.g., Bao and Hui, 1990; Bao and Zok, 1993) based on uniform crack bridging models. However, crack bridging in a functionally graded coating is non-uniform, since the local volume fraction of the metal phase changes with position in the coating.

In this study, crack bridging in the FGM coating is analyzed using a position-dependent crack bridging law. Considered is multiple cracking in a ceramic/metal FGM coating perfectly bonded to a homogeneous metal substrate, as depicted in Fig. 1. The coating is taken to be a composite with the local volume fraction of metal varying through the coating thickness according to a power-law type relation. Both the FGM coating and the metal substrate are taken as linear elastic; plastic deformation of the metal phase in the coating is included in the model through the crack bridging analysis. Systematic finite element predictions are made for the fracture driving force of bridged multiple cracks in a FGM coating as determined by the crack bridging characteristics, coating gradation, the crack length and spacing, and the applied load. Assuming the intrinsic toughness of the FGM coating is that of the ceramic phase, the onset of unstable crack growth and the crack arrest are also analyzed.

2. COATING GRADATION AND THE NON-UNIFORM CRACK BRIDGING

Based on the performance requirements for thermal barrier coatings and coatings in wear-related applications, in this study, only coatings that are ceramic-rich near the surface and metal-rich near the coating/substrate interface are considered. For convenience, the y-axis is set along the coating thickness direction, the x-axis lies within the coating/substrate interface, as illustrated in Fig. 1. At any position y in the ceramic/metal coating, the local volume fraction of ceramic is assumed to obey a pure power-law relation $g(y)$

$$g(y) = (y/h)^n \tag{1}$$

where the exponent n is a material parameter. The gradation given in (1) implies that the coating always has 100% ceramic at the coating surface (i.e., $g(h) = 1$) and 100% metal at the interface (i.e., $g(0) = 0$). The local volume fraction of metal $f(y)$ is given by

$$f(y) = 1-g(y) = 1-(y/h)^n \tag{2a}$$

and the total volume fraction of metal f_m in the coating is related to the exponent n in (1) by

$$f_m = n/(n+1). \tag{2b}$$

Due to the heterogeneous nature of a functionally graded material, it is quite difficult to obtain exact solutions of the effective elastic moduli of a FGM coating in terms of the relative volume fractions and elastic properties of the metal and ceramic phases. For a FGM coating of the inclusion/matrix type, the microgeometry of each phase is usually irregular, the spatial distribution of the phases is not uniform along the y-direction, and the homogenization can only be made within a plane parallel to the x-axis. Consequently, the existing micromechanical cell models are no longer valid since no unit cell containing a single inclusion can be used to represent the whole composite body. Even if one chooses a unit cell containing many particles aligned along the coating thickness direction, due to the finite thickness of the coating, there is a particle-size dependence of the unit cell. A robust micromechanical model for the thermomechanical properties of a functionally graded coating is yet to be developed (Markworth *et al.*, 1995).

As a first-order approximation, in this study, Young's modulus $E(y)$ and Poisson's ratio $v(y)$ of the FGM coating are obtained using micromechanics models developed for composites with homogeneously distributed spherical reinforcements. The effective bulk modulus $k(y)$ of the coating can be expressed as (Hashin, 1962)

$$k(y) = k_m + \frac{g(y)(k_c-k_m)}{1+[1-g(y)][(k_c-k_m)/(k_m+\frac{4}{3}\mu_m)]} \tag{3}$$

where k_m and k_c are bulk moduli for metal and ceramic, respectively, and μ_m is the shear modulus for the metal phase. The effective shear modulus $\mu(y)$ of the coating can be solved from (Christensen and Lo, 1979)

$$A\left[\frac{\mu(y)}{\mu_m}\right]^2 + B\left[\frac{\mu(y)}{\mu_m}\right] + C = 0 \tag{4}$$

where A, B and C are functions of $g(y)$, μ_c/μ_m, v_c and v_m (Poisson's ratios for ceramic and metal, respectively) given in Christensen and Lo (1979), and μ_c is the shear modulus for the ceramic phase. The effective Young's modulus $E(y)$ and Poisson's ratio $v(y)$ are given in terms of $k(y)$ and $\mu(y)$ by

$$E(y) = \frac{9k(y)\mu(y)}{3k(y)+\mu(y)}, \quad v(y) = \frac{E(y)}{2\mu(y)} - 1. \tag{5}$$

For a FGM coating that is ceramic-rich near the surface, cracks perpendicular to the interface can initiate at the coating surface and propagate into the coating under applied thermal or mechanical tensile loads (Lannutti, 1994). These cracks may be bridged by the

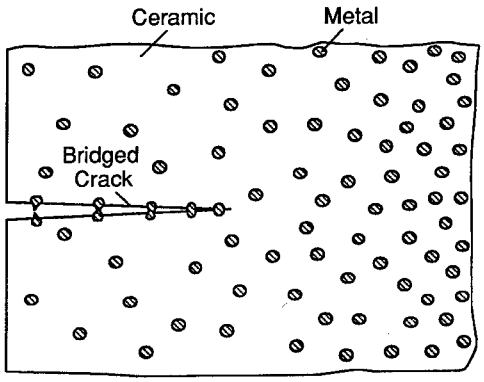

Fig. 2. A schematic of position-dependent crack bridging in functionally graded materials.

metal particle in the FGM coating, as shown schematically in Fig. 2. As a consequence of metal volume fraction variation in the FGM coating, the bridging traction on the crack surfaces provided by metal particles is position-dependent (Fig. 2). At a fixed location, the bridging-stress versus crack-opening curve for a single ductile particle bridging the matrix crack in its wake is typically as the solid line shown in Fig. 3a (Ashby *et al.*, 1989). To simplify the analysis and at the same time capture the essence of the bridging mechanism, in this study, an idealized rectilinear bridging law (Bao and Suo, 1992) shown as the dashed line in Fig. 3a will be used. Specifically, the rectilinear bridging law $\sigma(\delta)$ is characterized by two parameters σ_0 and δ_0

$$\sigma = \sigma_0, \quad 0 \leqslant \delta < \delta_0; \tag{6a}$$

$$\sigma = 0, \quad \sigma > \delta_0. \tag{6b}$$

In eqn (6), δ_0 can be chosen as the limiting separation of the crack surfaces beyond which the metal particle will rupture, and the bridging strength σ_0 can be given from the following energy-balance equation

$$\sigma_0 \delta_0 = \int_0^{\delta_0} \sigma(\delta)\, \mathrm{d}\delta \tag{6c}$$

where the function $\sigma(\delta)$ is the measured crack bridging curve shown as the solid line in Fig. 3a. In general, σ_0 depends on the plastic flow behavior and shape of the metal particles, and the particle/matrix interface strength (Mataga, 1989).

The crack bridging law given in (6) is for a single metal particle that bridges the crack. The crack bridging law shown in Fig. 3b for the entire bridging zone is obtained by smearing out the stresses in the bridging particles according to the local volume fraction of metal in the FGM coating

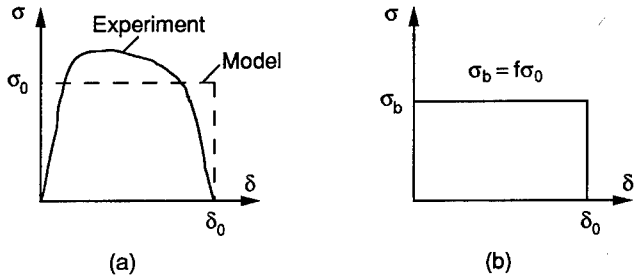

Fig. 3. The crack bridging law (a) for a single metal particle in the bridging zone; (b) for the FGM coating where f is the local volume fraction of the metal phase.

$$\sigma = \sigma_b, \quad 0 \leqslant \delta < \delta_0; \tag{7a}$$

$$\sigma = 0, \quad \delta > \delta_0 \tag{7b}$$

where $\sigma_b(y) = f(y)\sigma_0$ is the position-dependent bridging strength

$$\sigma_b(y) = [1-g(y)]\sigma_0 = [1-(y/h)^n]\sigma_0. \tag{7c}$$

In deriving eqn (7), it is assumed that the local area fraction of the bridged particles can be taken as the local volume fraction of metal phase. While not true for all cases, this assumption is valid for a large class of composites.

3. MULTIPLE CRACKING UNDER UNIFORM STRAINING

Analyzed in this section is multiple cracking in the FGM coating/metal substrate system owing to a remotely applied uniform strain ε_0 in the x-direction, as illustrated in Fig. 1. For simplicity, the cracks are taken to be mode I, plane strain, parallel and equally spaced with spacing $2L$, and have the same length. For an uncracked coating/substrate system subjected to ε_0, the stress along the x-direction in the coating is given by

$$\sigma_x(y) = \frac{\varepsilon_0 E(y)}{1-\nu^2(y)} \tag{8}$$

and that in the substrate is uniform

$$\sigma_x = \frac{\varepsilon_0 E_m}{1-\nu_m^2}. \tag{9}$$

The average stress in the x-direction corresponding to the applied strain ε_0 is obtained readily as

$$\sigma = \frac{\varepsilon_0}{h+H}\left[\frac{HE_m}{1-\nu_m^2} + \int_0^h \frac{E(y)}{1-\nu^2(y)}\,\mathrm{d}y\right] \tag{10}$$

where H is the thickness of the substrate. In what follows, this average stress σ, often referred to as the "applied stress", is used to represent the effect of the applied strain ε_0. The energy release rate $\mathscr{G}$ at each tip of the unbridged multiple cracks can be normalized to give

$$\frac{\mathscr{G}\bar{E}_m}{\sigma^2 h} = \psi\left(\frac{a}{h}, \frac{L}{h}, \frac{\delta_0}{h}, \frac{\sigma_0}{E_m}, \frac{\sigma}{E_m}, n\right) \tag{11}$$

where ψ is a non-dimensional function and the dependence of ψ on E_c/E_m, ν_c and ν_m is left implicit. Systematic finite element predictions are made for the energy release rate $\mathscr{G}$ at the tip of the bridged crack varying a/h, L/h, σ_0/E_m, σ/E_m and n. A detailed discussion of these predictions is given in Section 3.3.

3.1. *The finite element model*

Finite element calculations were carried out using the commercial code ABAQUS to obtain the energy release rate $\mathscr{G}$ for bridged multiple cracks in a FGM coating. The coating/substrate system depicted in Fig. 1 is subjected to a remotely applied uniform strain ε_0 in the x-direction. Owing to translational symmetry of the parallel cracks, only a unit

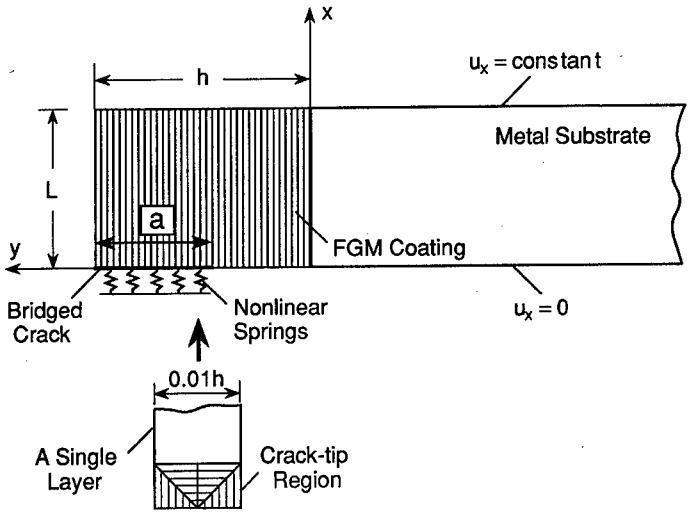

Fig. 4. The unit cell used in the finite element calculations for the bridged multiple cracks in the FGM coating. The coating is divided into 100 layers and the energy release rate is calculated with the crack tip located in the middle of a layer.

cell with width L containing a single crack as shown in Fig. 4 needs to be considered in the finite element calculation. The thickness of the substrate H is taken to be $300h$ where h is the coating thickness. The FGM coating is divided into 100 layers with one element per layer in the thickness direction, each layer is homogeneous, isotropic with elastic moduli $E(y_i)$ and $v(y_i)$ where y_i is the position of the middle plane of the layer measured from the coating/substrate interface ($y = 0$). Clearly, in this finite element model the gradation is not continuous, nor is it in the real material. This model mimics the microstructure of a fine multilayered FGM coating, or an inclusion/matrix type FGM coating with gradation $g(y)$.

As can be seen from Fig. 4, the mode I, plane strain crack lies on $x = 0$, $h-a \leqslant y \leqslant h$. For $-H \leqslant y \leqslant h-a$, the displacement in the x-direction $u_x = 0$. The unit cell is constrained in such a way that the edge $x = L$ has a uniform displacement in the x-direction $u_x = \varepsilon_0 L$, where ε_0 is the applied strain. The energy release rate is calculated with the crack tip located in the middle of a layer, as depicted in Fig. 4. Complications due to the singular behavior at the interfaces of two adjacent layers can thus be avoided. The position-dependent crack bridging is simulated using discrete nonlinear springs attached to the nodes on the crack surfaces and to the symmetry plane $x = 0$. The behavior of the nonlinear springs is defined by the relationship between the force and the relative displacement in the spring, i.e.,

$$P = \begin{cases} A_b\sigma_b = A_b\sigma_0[1-(y_i/h)^n], & \text{when } 0 \leqslant \delta < \delta_0 \\ 0, & \text{when } \delta \geqslant \delta_0 \end{cases} \tag{12}$$

where A_b is the element area (or length in the case of a plane strain problem) associated with the attached spring and y_i is the location of the middle plane of the layer containing the nonlinear spring. In all the finite element calculations, fixed values of $E_c/E_m = 3.0$, $v_c = 0.2$, $v_m = 0.3$, $\delta_0/h = 0.05$ were used. An accuracy check of this finite element crack bridging model has been carried out as discussed below.

3.2. *Validation of the finite element crack bridging model*

In order to check the accuracy of the finite element crack bridging model discussed above, a special case is considered in which the coating is taken to be homogeneous isotropic with elastic moduli identical to that of the substrate. The crack bridging law is taken to be rectilinear as defined in (7a) and (7b) with the position-dependent bridging strength σ_b given by

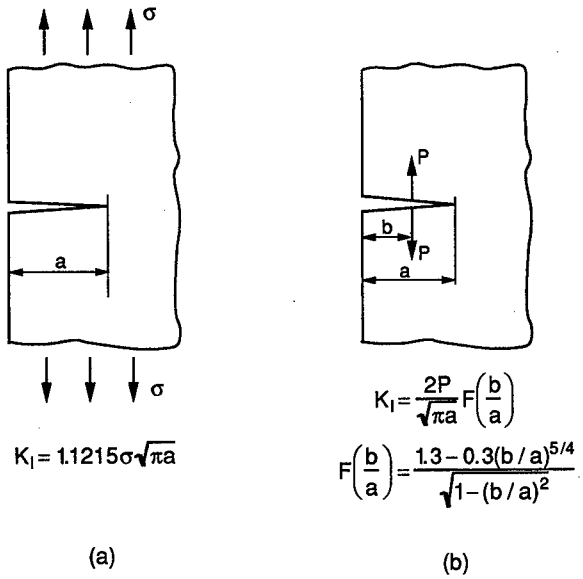

Fig. 5. The stress intensity factor for an edge crack in a semi-infinite homogeneous isotropic body under (a) remotely applied uniform stress and (b) a pair of point loads on the crack surfaces.

$$\sigma_b = (t/h)\sigma_0 \tag{13}$$

where t is the position in the coating measured from the coating surface, and h is the coating thickness. Evidently, eqn (13) is a special case of (7c) with $t = h-y$ and $n = 1$.

For a single unbridged edge crack with length a in a semi-infinite, homogeneous, isotropic body under remotely applied tensile stress σ as depicted in Fig. 5a, the stress intensity factor K_a is given by (Tada *et al.*, 1985)

$$K_a = 1.1215\sigma\sqrt{\pi a}. \tag{14}$$

On the other hand, the stress intensity factor of the crack under a pair of point loads P applied on the crack surfaces a distance b away from the coating surface (Fig. 5b) is given by (Tada *et al.*, 1985)

$$K_I = \frac{2P}{\sqrt{\pi a}} F\left(\frac{b}{a}\right) \tag{15a}$$

where

$$F\left(\frac{b}{a}\right) = \frac{1.3-0.3(b/a)^{5/4}}{\sqrt{1-(b/a)^2}}. \tag{15b}$$

The crack-tip stress intensity K_{tip} for a fully bridged crack is thus

$$K_{tip} = 1.1215\sigma\sqrt{\pi a} - \frac{2}{\sqrt{\pi a}}\int_0^a \sigma_b(t) F\left(\frac{t}{a}\right) dt. \tag{16}$$

Substituting (13) into (16) and performing the integration, we have

$$\frac{K_{tip}}{\sigma\sqrt{\pi a}} = \left(1.1215 - \frac{2.15}{\pi}\frac{\sigma_0}{\sigma}\frac{a}{h}\right). \tag{17}$$

In a nondimensional form, the energy release rate $\mathcal{G}$ at the crack-tip can be expressed as

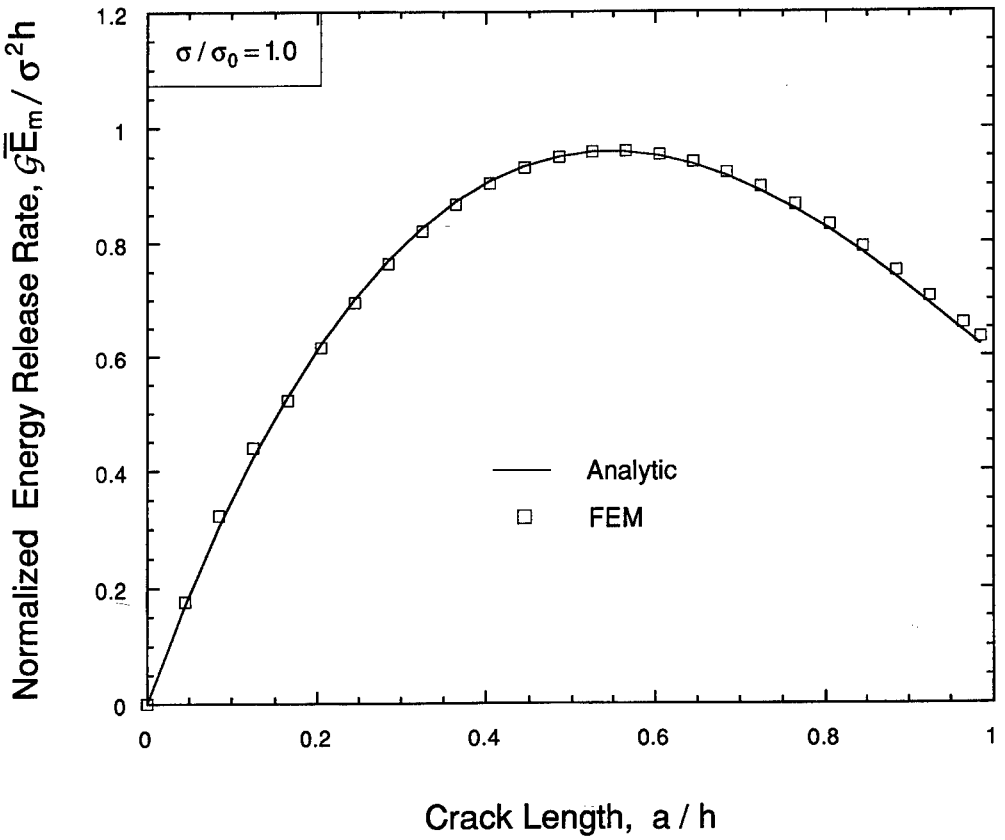

Fig. 6. Comparison of the normalized crack-tip energy release rate as a function of the crack length obtained using the closed-form solution (18) and the finite element crack bridging model.

$$\frac{\mathcal{G}\bar{E}_m}{\sigma^2 h} = \pi\left(1.1215 - \frac{2.15}{\pi}\frac{\sigma_0}{\sigma}\frac{a}{h}\right)^2 \frac{a}{h} \tag{18}$$

where $\bar{E}_m = E_m/(1-\nu_m^2)$ is the plane strain Young's modulus of the substrate.

Plotted in Fig. 6 is the comparison of the normalized energy release rate as a function of the crack length obtained from the closed-form solution (18) and from the finite element calculations with $\sigma_0/E_m = 0.001$ under applied stress $\sigma/E_m = 0.001$. In the finite element calculations, $L/h = 100$, $H/h = 300$ is used. The limiting-separation δ_0 assumed in the crack bridging law is sufficiently large ($\delta_0/h = 0.05$) so that the crack remains fully bridged under the applied load. As can be seen from the comparison shown in Fig. 6, the finite element model is quite accurate in obtaining the energy release rate of a bridged crack.

3.3. *Finite element predictions*

Plotted in Fig. 7 is the normalized energy release rate $\mathcal{G}\bar{E}_m/\sigma^2 h$ as a function of the normalized crack length a/h with $n = 1$, $\sigma_0/E_m = 0.002$, $L/h = 2$ under applied stress $\sigma/E_m = 0.0004$. Corresponding results for multiple cracks in a pure ceramic coating and unbridged cracks in the FGM coating are also shown for comparison. It is clear that FGM coatings can significantly reduce the crack driving force and crack bridging can make the driving force reduction even more pronounced. In particular, for the bridged cracks, the energy release rate versus crack length curve shows a peak indicating that the cracks may arrest at a certain crack length when the fracture driving force falls below the intrinsic toughness of the coating and thereafter, an increased applied load is required to propagate the crack further (stable crack growth). This scenario will be discussed in more detail in Section 4. It is also noteworthy that for the bridged crack, the energy release rate $\mathcal{G}$ at the crack tip goes to zero at about $a = 0.6h$. This is due to the fact that the applied load is

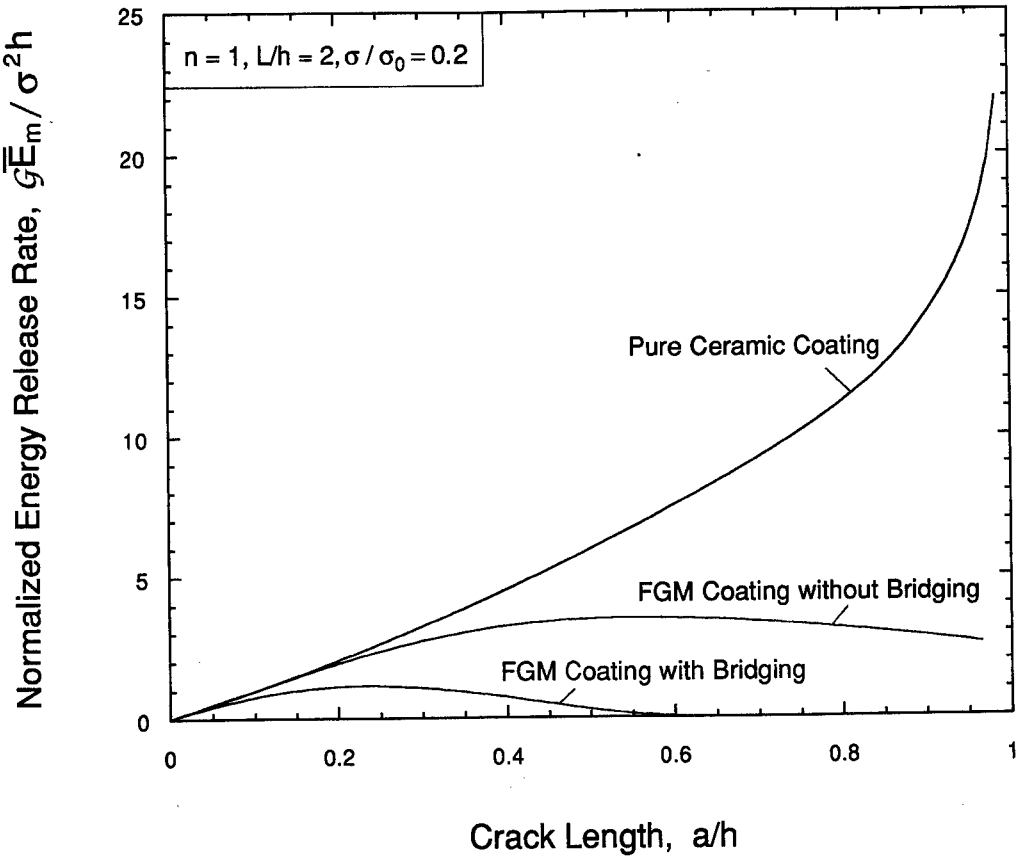

Fig. 7. Comparison of the normalized energy release rates as a function of the crack length for (i) unbridged cracks in a pure ceramic coating; (ii) unbridged cracks in a FGM coating; and (iii) bridged cracks in a FGM coating.

relatively low, and the crack bridging is quite strong; the crack is always fully bridged since the assumed limiting-separation δ_0 is large.

To uncover the influence of coating gradation on the fracture driving force, systematic predictions are made for the energy release rate $\mathcal{G}$ corresponding to different coating gradation $g(y)$. Shown in Fig. 8 are $\mathcal{G}\bar{E}_m/\sigma^2 h$ vs a/h curves for $L/h = 2$, $\sigma_0/E_m = 0.002$, $\sigma/E_m = 0.0005$ for $n = 0.5$, 1 and 2. As expected, there is a strong dependence of $\mathcal{G}$ on the value of gradation exponent n: a large value of n leads to a low energy release rate $\mathcal{G}$. Note that a large n implies a high metal content in the coating, as indicated by eqn (2b).

The effect of bridging strength σ_0 is illustrated in Fig. 9 in which $\mathcal{G}\bar{E}_m/\sigma^2 h$ is plotted as a function of a/h for $n = 1$, $L/h = 2$, $\sigma/E_m = 0.0004$ for $\sigma_0/E_m = 0.001$, 0.002, 0.003. The trend is clear: a high bridging strength σ_0 gives a low fracture driving force. In fact, with a fixed crack opening δ at the coating surface the reduction in crack-tip energy release rate due to plastic deformation of the bridging metal particles is simply proportional to σ_0. Note also that the crack length at which the energy release rate $\mathcal{G}$ approaches zero decreases with increasing σ_0.

Presented in Fig. 10 is $\mathcal{G}\bar{E}_m/\sigma^2 h$ as a function of the crack length a/h for $n = 1$, $\sigma/E_m = 0.0004$, $\sigma_0/E_m = 0.002$ for $L/h = 2$, 5, 10 and 50. The energy release rate $\mathcal{G}$ increases with crack spacing, or in other words, the fracture driving force for each crack is reduced as more and more cracks developed (i.e., L/h becomes smaller). It is interesting to note that when the crack length is small (say, $a/h < 0.2$), the energy release rate is essentially independent of crack spacing. It is also clear that when crack spacing L/h becomes large (say, $L/h > 50$), the interaction between the parallel cracks diminishes, and each crack behaves like an isolated crack. That is the reason behind the saturating trend of the effect of L/h on energy release rate $\mathcal{G}$ as shown in Fig. 10.

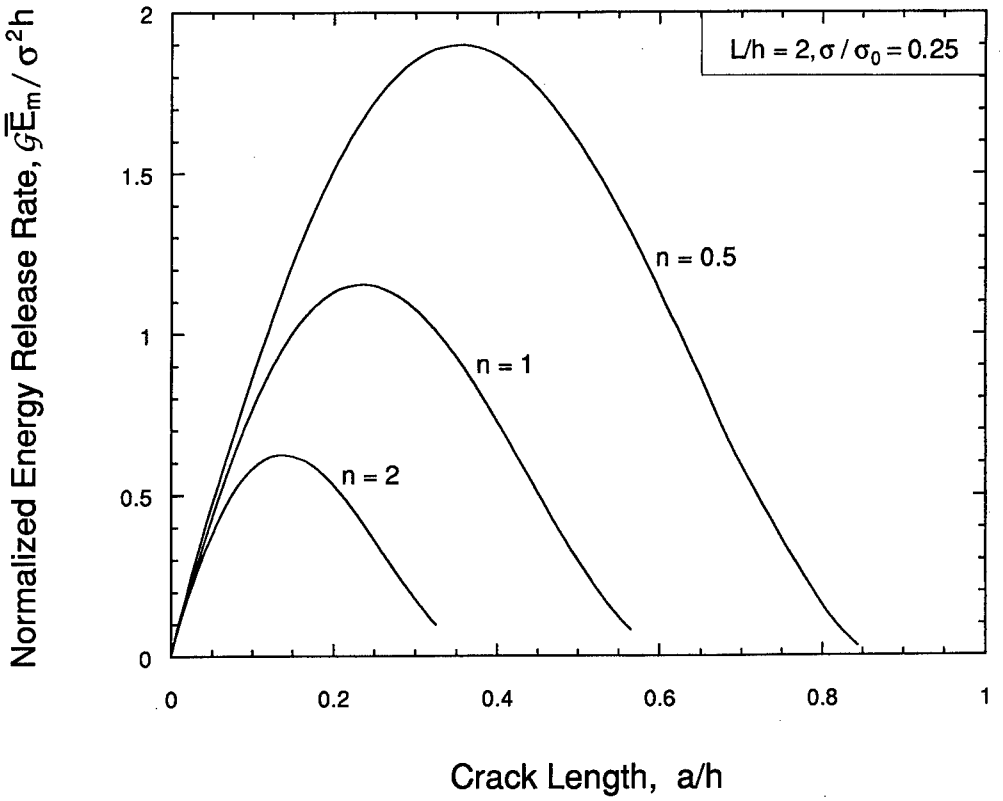

Fig. 8. The normalized energy release rate as a function of the crack length for FGM coatings with $n = 0.5$, 1.0 and 2.0, $L/h = 2$, $\sigma_0/E_m = 0.002$ under applied stress $\sigma/E_m = 0.0004$.

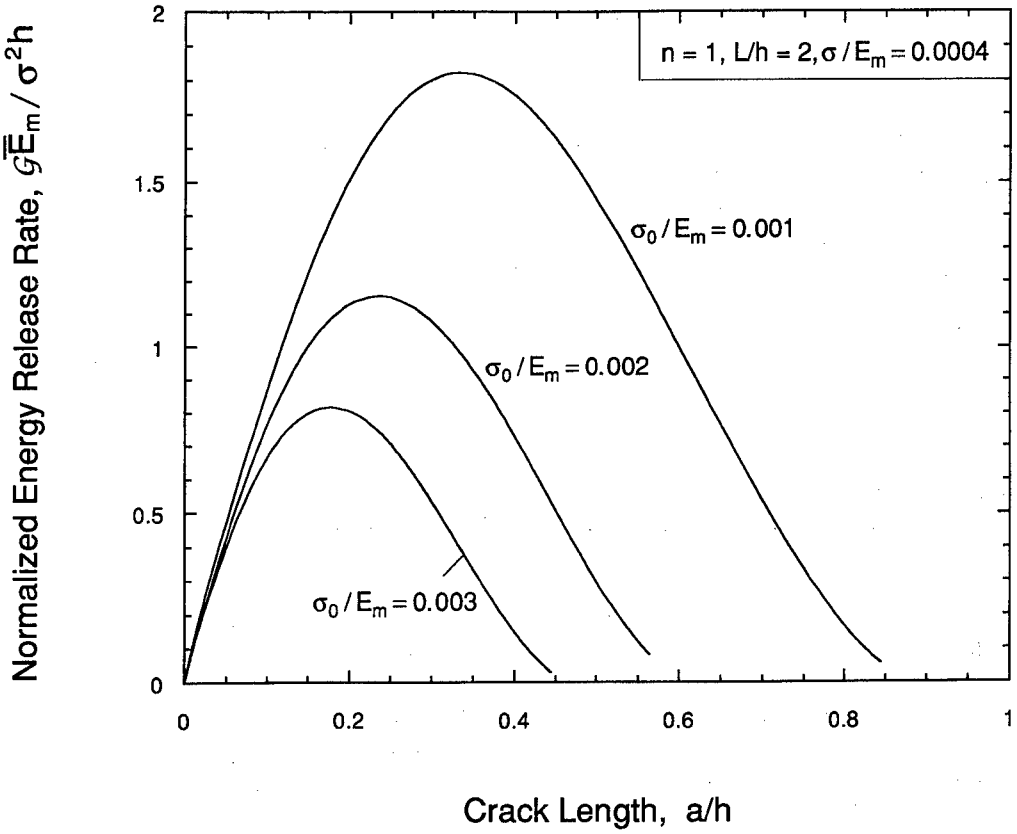

Fig. 9. The normalized energy release rate as a function of the crack length for FGM coatings with $n = 1$, $L/h = 2$, $\sigma_0/E_m = 0.001$, 0.002 and 0.003 under applied stress $\sigma/E_m = 0.0004$.

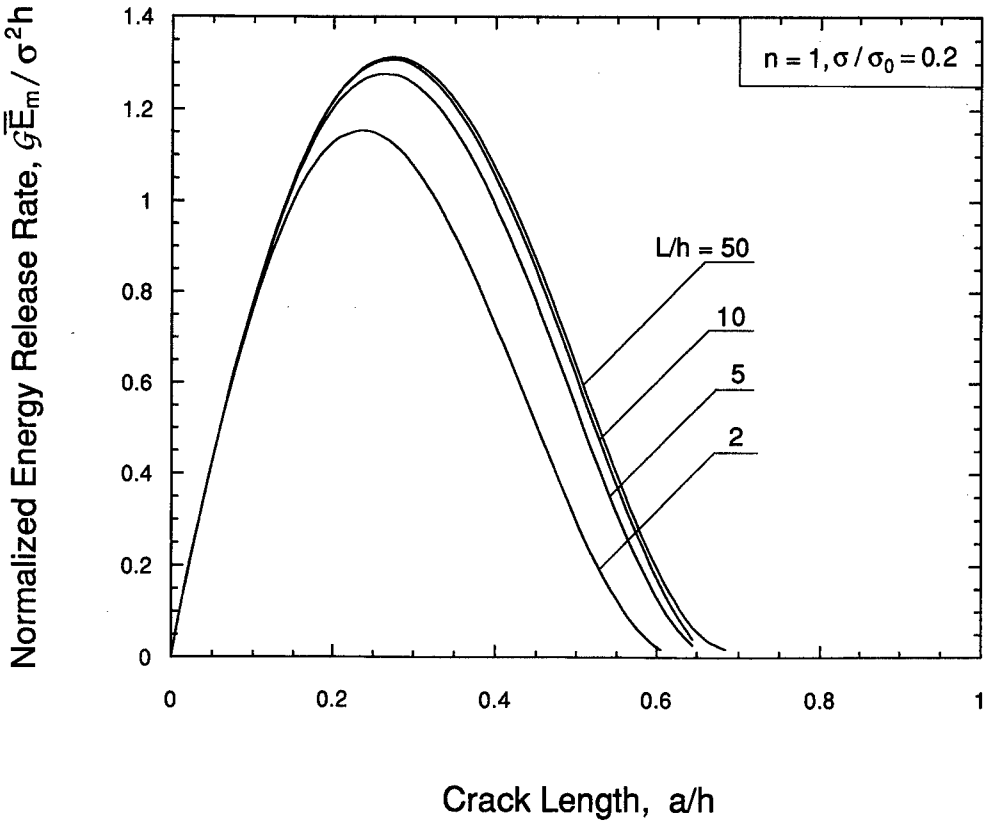

Fig. 10. The normalized energy release rate as a function of the crack length for a FGM coating with $n = 1$, $L/h = 2$, 5, 10 and 50, $\sigma_0/E_m = 0.002$ under applied stress $\sigma/E_m = 0.0004$.

Figure 11 shows the normalized energy release rate $\mathcal{G}\bar{E}_m/\sigma^2 h$ as a function of the crack length a/h for $n = 1$, $L/h = 2$, $\sigma_0/E_m = 0.002$ for different applied load $\sigma/E_m = 0.0003$, 0.0004, 0.0005. Evidently, the fracture driving force $\mathcal{G}$ increases with applied load. However, the crack-tip energy release rate $\mathcal{G}$ does not scale with σ^2 as for an unbridged crack due to the nonlinear feature of the crack bridging and the interplay between crack bridging and the applied load. Otherwise, all the curves shown in Fig. 11 should collapse onto one curve.

The $\mathcal{G}\bar{E}_m/\sigma^2 h$ vs a/h curves shown in Figs 8–11 indicate that, under the given applied far-field uniform strain ε_0, the energy release rate $\mathcal{G}$ at the crack-tip may become zero at certain crack length. This can be understood from the following energy equation

$$\mathcal{G} = \mathcal{G}_{\text{appl}} - \mathcal{G}_b \tag{19}$$

where $\mathcal{G}_{\text{appl}}$ and $\mathcal{G}_b$ are the energy release rates due to the applied strain ε_0 and crack bridging, respectively. Owing to the functional gradation of the coating, for $a/h > 0.2$, $\mathcal{G}_{\text{appl}}$ does not change much with crack length as can be seen from Fig. 7, but $\mathcal{G}_b$ increases as the crack length a increases. At certain crack length say, $a = a_c$, $\mathcal{G}_b$ may become the same as $\mathcal{G}_{\text{appl}}$, which implies that at a_c the crack-tip energy release rate $\mathcal{G}$ is zero.

4. STABLE CRACK GROWTH IN A FGM COATING

As mentioned earlier, the fracture driving force vs crack length curve for bridged multiple cracks in a functionally graded coating has a peak indicating that a crack may initiate at certain crack length and arrest at another under a given applied load. Based on the finite element results for the crack-tip energy release rate discussed in the last section, and the intrinsic toughness of the coating, the crack length at the onset of unstable crack growth and the crack length at arrest can be quantified.

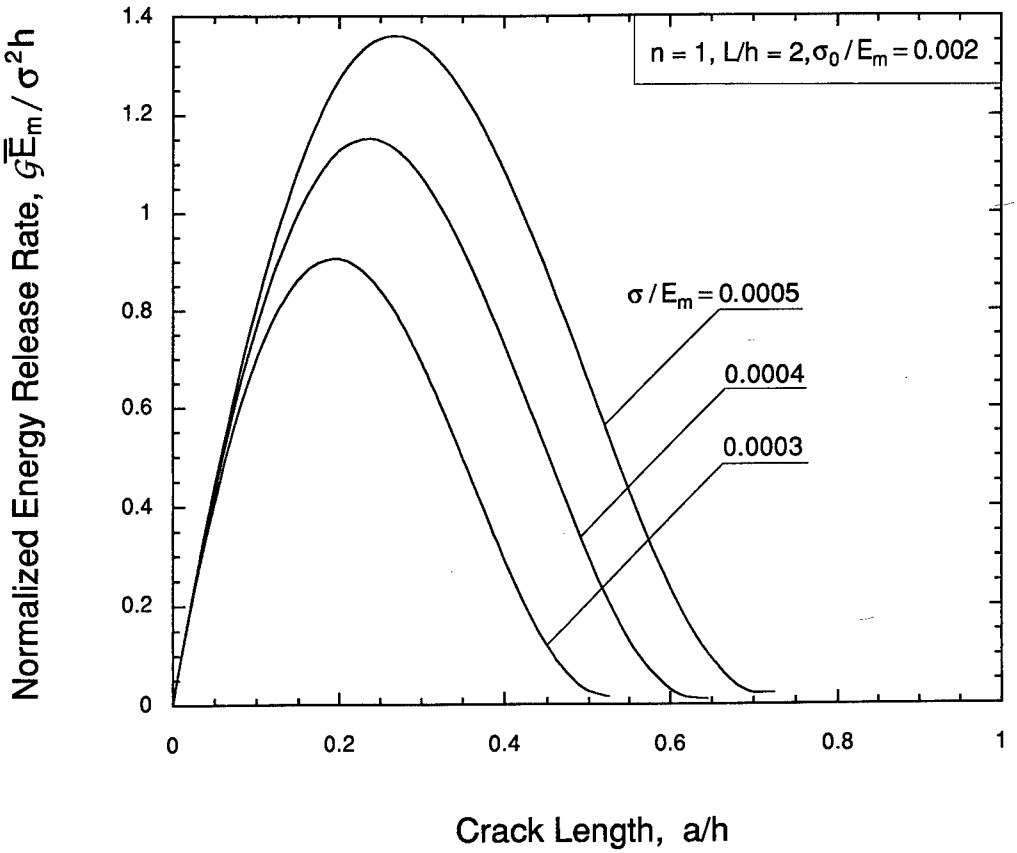

Fig. 11. The normalized energy release rate as a function of the crack length for a FGM coating with $n = 1$, $L/h = 2$, $\sigma_0/E_m = 0.002$ under applied stresses $\sigma/E_m = 0.0003$, 0.0004 and 0.0005.

4.1. *Intrinsic toughness of a FGM coating*

As a ceramic/metal composite, the toughness of a FGM coating is in general determined by the toughness of both the ceramic and the metal phases. However, compared with the metal phase, the ceramic phase in a FGM coating experiences larger stresses under a uniform applied strain field, but its toughness is much lower. Therefore, the ceramic phase in the coating always fractures first. In this study, we assume that in the ceramic-rich region of the coating, the cracks are in the ceramic matrix; metal particles contribute to the coating toughness only through crack bridging, as illustrated in Fig. 12. Further, in the metal-rich region, the crack length is so defined such that the fractured ceramic particles lying within the major crack plane are included (Fig. 12). Specifically, the crack tip is assumed to be located at the breaks of the ceramic particles, and the metal matrix in the crack plane behind the crack-tip is modeled as the bridging material. This approach is analogous to the cohesive zone model used by Rice (1968) for crack growth in a metal under small-scale yielding conditions. We thus define the *intrinsic toughness* of a FGM coating as that of the ceramic phase; the contribution of metal phase to the coating toughness is reflected by the reduction in the crack-tip energy release rate $\mathcal{G}$ due to crack bridging. From the viewpoint of energy balance concerning crack growth, both approaches, i.e., either counting bridging as a toughness enhancer or as a driving force reducer, are equivalent.

Assume that the toughness of the ceramic phase is Γ_c. For typical ceramic/metal combinations for advanced composite materials, the normalized intrinsic toughness of the coating $\Gamma_c/E_m h$ can range from 1.0×10^{-7} to 1.0×10^{-5} (Ashby and Jones, 1980). To gain insight into the stable crack growth in a FGM coating, in the following discussions, the material system consisting of SiC/Ti FGM coating on a Ti substrate will be considered as an example. Since for silicon carbide (SiC), toughness $K_c = 3$ MPa$\sqrt{\text{m}}$, Young's modulus $E_c = 450$ GPa, and for titanium (Ti), $E_m = 116$ GPa (Ashby and Jones, 1980), we have $\Gamma_c/E_m h = 1.66\times10^{-7}$ for a SiC/Ti coating with 1 mm thickness. For material systems other

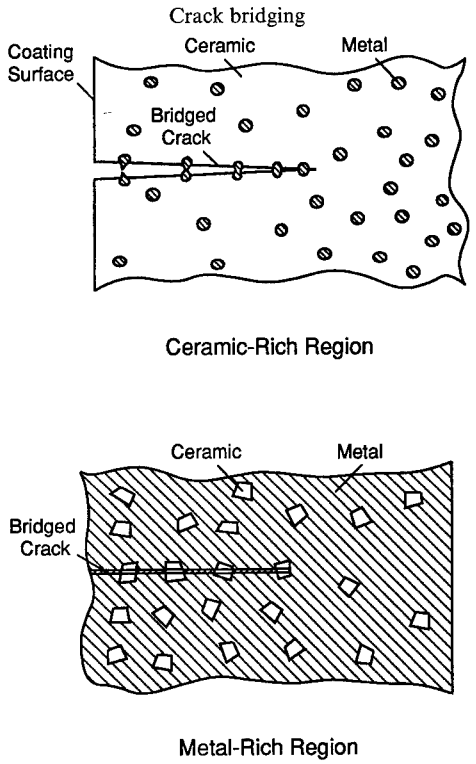

Fig. 12. A schematic showing crack bridging in different regions in the FGM coating. The crack tip is always in the ceramic phase and the intrinsic toughness of the coating is assumed to be that of the ceramic.

than the SiC/Ti considered here, the same approach can be taken in predicting the stable crack growth in a FGM coating.

4.2. *Stable crack growth in a FGM coating*

Unstable crack growth is a common feature for brittle materials such as ceramics of which the toughness is a constant independent of the crack length. However, the fracture driving force is usually a monotonic increasing function of crack length. Hence, once the crack starts to grow the whole structure or component ruptures since the fracture driving force is always higher than the toughness after the crack growth initiates at

$$\mathcal{G} = \Gamma_c \tag{20}$$

where $\mathcal{G}$ is the fracture driving force and Γ_c is the material toughness.

In contrast to unstable crack growth, stable crack growth implies that an increased applied load is necessary to propagate the crack further. For bridged multiple cracks in a FGM coating, under a given applied load, the fracture driving force $\mathcal{G}$ increases with crack length at the beginning, reaches the peak value, then decreases with crack length. Consequently, even if the crack starts to grow under a given applied load, the crack may arrest at certain crack length. Once the crack arrests, an increase in the applied load is required for further crack growth.

Shown in Fig. 13a is a typical energy release rate $\mathcal{G}\bar{E}_m/\sigma^2 h$ vs crack length a/h curve along with the intrinsic toughness of the coating $\Gamma_c\bar{E}_m/\sigma^2 h$ represented by the horizontal line, which intersects the driving force curve at crack lengths a_i and a_s. These two points have special meaning and importance: a_i corresponds to the critical initial crack length beyond which crack growth starts and a_s is the crack length at arrest. Under a given applied load, if the initial crack size is smaller than a_i the crack will not grow because the fracture driving force is lower than the toughness. On the other hand, if the initial crack size is between a_i and a_s, the crack will grow, and eventually arrest at $a = a_s$.

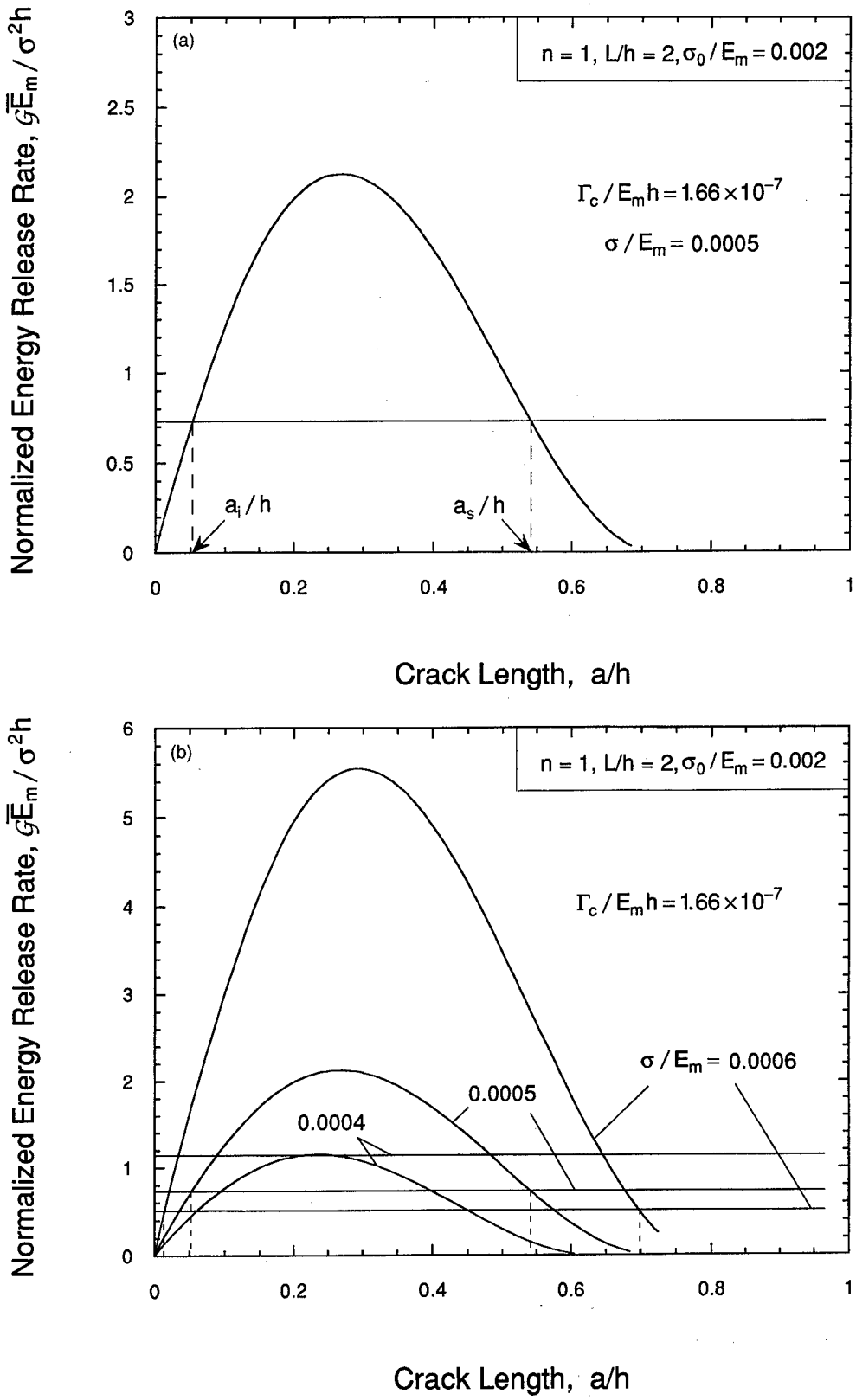

Fig. 13. Energy release rate as a function of the crack length together with the intrinsic toughness of the coating. (a) Under a given applied load, the crack starts to grow if $a \geqslant a_i$, and arrests at $a = a_s$. (b) With different applied loads, the crack has different critical initial crack length a_i and crack length at arrest a_s.

To further illustrate the trends in crack growth, in Fig. 13b curves of energy release rate $\mathscr{G}\bar{E}_m/\sigma^2 h$ vs crack length a/h are plotted together with the intrinsic toughness of the coating $\Gamma_c\bar{E}_m/\sigma^2 h$ represented by the horizontal lines for $n = 1$, $L/h = 2$, $\sigma_0/E_m = 0.002$ for $\sigma/E_m = 0.0004$, 0.0005 and 0.0006. Note that the intrinsic toughness of the coating is assumed to be $\Gamma_c/E_m h = 1.66 \times 10^{-7}$ and different horizontal lines representing $\Gamma_c\bar{E}_m/\sigma^2 h$ correspond to different values of the applied load used in calculating the energy release rate $\mathscr{G}$. Evidently, when the applied load is low, say, $\sigma/E_m = 0.0004$, the whole curve of fracture driving force $\mathscr{G}$ falls below the toughness curve Γ_c; crack growth is thus prohibited. Under a larger applied load, say, $\sigma/E_m = 0.0005$, the multiple cracks grow when their length $a \geqslant 0.05h$, and arrest at about $a = 0.54h$. At an even higher load, $\sigma/E_m = 0.0006$, the cracks start to grow at $a \approx 0.01h$ and stop at $a = 0.7h$. As expected, beyond certain crack length, further crack growth in the coating requires an increase in the applied load.

As discussed in the previous section, the fracture driving force $\mathscr{G}$ for bridged multiple cracks in the FGM coating depends on coating gradation as well as the crack bridging characteristics. In general, under a given applied load, the crack length at arrest a_s increases with decreasing n and σ_0/E_m, as can be seen from the curves in Figs 8 and 9. The influence of n and σ_0/E_m on the critical initial crack length a_i is found to be relatively insignificant.

5. CONCLUDING REMARKS

Functionally graded ceramic/metal coatings can have fracture toughness much higher than the pure ceramic coating due to the plastic deformation of the metal phase in the coating. Thus, cracks initiated at the coating surface and propagating perpendicular to the coating/substrate interface must overcome greater resistance. Specifically, in the ceramic-rich region of the coating, metal ligaments in the crack wake bridge the crack; in the metal-rich region, plastic deformation of the metal matrix near the crack tip consumes energy. To quantify the effect of crack bridging and plastic deformation on crack growth in the FGM coating, in this article, a finite element model for multiple cracking in FGM coating/metal substrate systems is developed based on a position-dependent crack bridging law. The influence of material and mechanics parameters such as coating gradation, bridging strength, crack length and spacing, and applied load on the crack tip energy release rate is studied systematically. Though relatively simple, the crack bridging analysis given in this paper can provide a basis for further studies of the fracture toughness of functionally graded materials.

The finite element results reveal that the coating gradation exponent n can have significant effects on the fracture driving force and the crack length at arrest: under fixed applied load, a larger value of n (i.e., higher metal content in the coating) gives a lower energy release rate $\mathscr{G}$ and a smaller crack length at arrest a_s. Further, with the same coating gradation, a high bridging strength σ_0 leads to a large reduction in the fracture driving force and the crack length at arrest. However, coating gradation, crack spacing, and bridging strength have very limited effects on the critical initial crack length a_i.

In this study we assume that the ductility δ_0 of the bridging material (the separation of the crack surfaces at particle rupture) and the intrinsic toughness of the coating Γ_c do not change with position in the coating. However, in reality, the crack bridging parameters σ_b and δ_0, and the intrinsic toughness Γ_c may all be position-dependent. Usually δ_0 is influenced by the size and shape of the metal particles which may change as the local volume fraction of metal in the coating varies. Further, the intrinsic toughness Γ_c—defined as the toughness of the ceramic phase—may depend on microcracking in the ceramic phase, and the thermal residual stresses. The precise position-dependence of σ_b may also be more complicated than that assumed in this article ($\sigma_b(y) = [1-(y/h)^n]\sigma_0$), since σ_0 may be different in the ceramic-rich region where the metal particles are surrounded by the ceramic matrix, and in the metal-rich region where the metal is the continuous phase. All these issues will be addressed in the subsequent studies of the fracture resistance of functionally graded materials.

The finite element crack bridging model developed in this study is based on several assumptions which render the model to be applicable only for crack lengths $a \leqslant 0.7h$. First,

the limiting separation of the crack bridging is taken to be $\delta_0 = 0.05h$ which is quite large. Consequently, in all the finite element calculations, the crack remains fully bridged. This may have overestimated the effect of crack bridging when the crack length becomes large. Further, the plastic deformation of metal in the metal-rich region of the FGM coating is taken into account through the position-dependent crack bridging law by assuming that the crack tip is located at the fractured ceramic particles in the crack plane. A consequence of this approach is that the model predictions are less accurate for crack lengths much larger than $0.6h$. This model, similar to the cohesive-zone model used by Rice (1968), is valid only if the plastic yielding is of small scale. For large-scale yielding cases, the present finite element model can be extended readily to fully reflect the effect of plastic deformation on crack growth in a FGM coating by taking the metal-rich region of the FGM coating and the metal substrate to be elastoplastic materials. Such an extension is left for future studies.

Acknowledgement—This work was supported by AFOSR through a research grant F49620-95-1-0120 to G. Bao.

REFERENCES

Aboudi, J., Arnold, S. M. and Pindera, M. J. (1994) Response of functionally graded composites to thermal gradients. *Composites Engineering* **4,** 1–18.

Ashby, M. F., Blunt, F. J. and Bannister, M. (1989) Flow characteristics of highly constrained metal wires, *Acta Metallica* **37,** 1847–1857.

Ashby, M. F. and Jones, D. R. H. (1980) *Engineering Materials* 1, Pergamon Press, New York.

Bao, G. and Cai, H. (1997) Delamination cracking in functionally graded coating/metal substrate systems. *Acta Materiala* **45,** 1055–1066.

Bao, G. and Hui, C. Y. (1990) Effects of interface debonding on the toughness of ductile-particle reinforced ceramics. *International Journal of Solids and Structures* **26,** 631–642.

Bao, G. and McMeeking, R. M. (1994) Fatigue crack growth in fiber reinforced metal matrix composites. *Acta Metallica Materiala* **42,** 2415–2425.

Bao, G. and McMeeking, R. M. (1995) Thermomechanical fatigue cracking in fiber reinforced metal-matrix composites. *Journal of the Mechanics and Physics of Solids* **43,** 1433–1460.

Bao, G. and Suo, Z. (1992) Remarks on crack bridging concepts. *Applied Mechanics Review* **45,** 355–366.

Bao, G. and Wang, L. (1995) Multiple cracking in functionally graded ceramic/metal coatings. *International Journal of Solids and Structures* **32,** 2853–2871.

Bao, G. and Zok, F. W. (1993) On the strength of ductile particle reinforced brittle matrix composites. *Acta Metallica Materiala* **41,** 3515–3524.

Chen, Y. F. and Erdogan, F. (1996) The interface crack problem for a non-homogeneous coating bonded to a homogeneous substrate. *Journal of the Mechanics and Physics of Solids* **44,** 771–787.

Christensen, R. M. and Lo, K. H. (1979) Solutions for effective shear properties in three phase sphere and cylinder models. *Journal of the Mechanics and Physics of Solids* **27,** 315–330.

Delale, F. and Erdogan, F. (1983) The crack problem for a nonhomogeneous plane. *Journal of Applied Mechanics* **50,** 609–614.

Delale, F. and Erdogan, F. (1988) On the mechanical modeling of the interface region in bonded half-planes. *Journal of Applied Mechanics* **55,** 317–324.

Drake, J. T., Williamson and Rabin, R. L., (1993) Finite element analysis of thermal residual stresses at graded ceramic-metal interfaces. Part II. Interface optimization for residual stress reduction. *Journal of Applied Physics* **74,** 1321–1326.

Dvorak, G. and Zuiker, J. (1994) The effective properties of functionally graded composites I. Extension of the Mori-Tanaka method to linearly varying fields. *Composites Engineering* **4,** 19–35.

Erdogan, F. (1985) The crack problem for bonded nonhomogeneous materials under antiplane shear loading. *Journal of Applied Mechanics* **52,** 823–828.

Erdogan, F. and Wu, B. H. (1993) Analysis of FGM specimens for fracture toughness testing. In *Ceramic Transactions,* Vol. 34: Functionally Gradient Materials, eds J. B. Hole *et al.*, pp. 39–46. American Ceramic Society, Westerville, Ohio.

Finot, M. and Suresh, S. (1996) Small and large deformation of thick and thin-film multi-layers: effects of layer geometry, plasticity and compositional gradients. *Journal of Mechanics and Physics of Solids* **44,** 683–721.

Giannakopoulos, A. E., Suresh, S., Finot, M. and Olsson, M. (1994) Elastoplastic analysis of thermal cycling: Layered materials with compositional gradients. *Acta Metallica Materiala* **43,** 1335–1354.

Hashin, Z. (1962) The elastic moduli of heterogeneous materials. *Journal of Applied Mechanics* **29,** 143–150.

Jin, Z.-H. and Noda, N. (1993) An internal crack parallel to the boundary of a nonhomogeneous half plane under thermal loading. *International Journal of Engineering Science* **31,** 793–806.

Jin, Z.-H. and Noda, N. (1994) Transient thermal stress intensity factors for a crack in a semi-infinite plate of a functionally gradient material. *International Journal of Solids and Structures* **31,** 203–218.

Kokini, K. and Takeuchi, Y. (1994) Transient thermal fracture of an interface crack in the presence of a surface crack. *Journal of Thermal Stresses* **17,** 63–74.

Lannutti, J. J. (1994) Functionally graded materials: properties, potential and design guidelines. *Composites Engineering* **4,** 81–94.

Markworth, A. J., Ramesh, K. S. and parks, W. P. Jr. (1995) Modelling studies applied to functionally graded materials. *Journal of Material Science* **30,** 2183–2193.

Mataga, P. A. (1989) Deformation of crack-bridging ductile reinforcements in tough brittle materials. *Acta Metallica* **37,** 3349.

Mortensen A. and Suresh, S. (1995) Functionally graded metals and metal-ceramic composites : Part I. Processing. *International Materials Reviews* (submitted).

Noda, N. and Jin, Z.-H. (1993) Thermal stress intensity factors for a crack in a strip of a functionally gradient material. *International Journal of Solids and Structures* **30,** 1039–1056.

Rice, J. R. (1968) Mathematical Analysis in the Mechanics of Fracture. In *Fracture—An Advanced Treatise, Vol. II,* ed. H. Liebowitz. Academic, New York, pp. 191–308.

Tada, H., Paris, P. C. and Irwin, G. R. (1985) *The Stress Analysis of Cracks Handbook.* Del Research, Hellertown, PA.

Takahashi, H. and Hashida, T. (1990) Development of an evaluation method of functionally gradient materials. *JSME International Journal* **33,** 281–287.

Walls, D. P., Bao, G. and Zok, F. W. (1993) Mode I fatigue cracking in a fiber reinforced metal matrix composite. *Acta Metallica Materiala* **41,** 2061–2071.

Williamson, R. L., Rabin, B. H. and Drake, J. T. (1993) Finite element analysis of thermal residual stresses at graded ceramic-metal interfaces. Part I. Model description and geometrical effects. *Journal of Applied Physics* **74,** 1310–1320.